Smart Materials and Devices

Science Exploration

Open Access Mini Review

3D carbon-based MXene composite electrodes for supercapacitors: Synthesis strategies, hybrid architectures, and machine-learning-guided design

Boyuan Mu[1,2,*], Zhibin Hou[1], Shuhan Shi[1]

[1]Guangxi Key Laboratory of Functional Information Materials and Intelligent Information Processing, Nanning Normal University, Nanning 530100, Guangxi, China.
[2]School of Mechanical and Aerospace Engineering, Queen's University Belfast, Belfast BT9 5AH, UK.

***Correspondence to:** Boyuan Mu, School of Mechanical and Aerospace Engineering, Queen's University Belfast, Belfast BT9 5AH, UK. E-mail: boyuanmu@nnnu.edu.cn

Received: April 30, 2026 **Accepted:** July 07, 2026 **Published:** July 07, 2026

Cite this article: Mu B, Hou Z, Shi S. 3D carbon-based MXene composite electrodes for supercapacitors: Synthesis strategies, hybrid architectures, and machine-learning-guided design. Smart Mater Devices. 2026;2:202624. https://doi.org/10.70401/smd.2026.0038

Abstract

Supercapacitors (SCs) are critical for high-power energy storage, yet their practical deployment is still limited by insufficient energy density. MXenes have emerged as promising electrode materials owing to inherent metallic conductivity, hydrophilic terminations, and intercalation pseudocapacitance, but suffer from layer restacking and oxidative degradation. Hybridizing MXenes with 3D carbon scaffolds offers a synergistic strategy by providing interlayer spacers, hierarchical ion transport pathways, and oxidation barriers. To the best of our knowledge, this review is the first to systematically couple the structural design of MXene/3D-carbon composites with machine learning (ML) guided optimization, summarizing recent advances in MXene/3D-carbon composite electrodes. This review systematically evaluates MXene etching routes and representative composite assembly strategies, and classifies existing systems into three structural categories, critically comparing their performance metrics, strengths, and inherent limitations. It further highlights the frontier applications of ML in performance prediction, compositional optimization, and mechanical design, along with current challenges, including data bias, the black-box nature of models, and the gap between idealized predictions and real synthesis. Overall, this work aims to provide a framework for integrating advanced synthesis strategies, 3D architectures, and data-driven tools toward the rational design of high-performance SCs.

Keywords: MXene, 3D carbon materials, supercapacitor, composite electrode, machine learning

1. Introduction

The rapid growth of renewable energy generation and portable electronics has placed increasing demand on high-performance energy storage devices[1,2]. Supercapacitors (SCs), as a new generation of energy storage devices, have attracted significant attention. They overcome the limitations of traditional batteries in instantaneous power output and effectively balance energy and power density, making them promising candidates for addressing global energy shortages. However, compared with conventional batteries, SCs still suffer from relatively low energy density, limiting their ability to replace batteries in many applications and often confining them to auxiliary roles. Conventional carbon-based electric double-layer (EDL) capacitors exhibit excellent cycling stability but generally suffer from low specific capacitance and energy density. In contrast, pseudocapacitive materials offer high theoretical capacitance but are limited by poor electrical conductivity, restricted rate capability, and insufficient cycling stability. Therefore, the development of novel electrode materials that simultaneously achieve high electrical conductivity and high electrochemical activity is critical for overcoming the energy density limitations of SCs[3].

Various two-dimensional (2D) materials, hexagonal boron nitride (BN), hydroxides, carbon-based materials, MXenes, and transition-metal oxides, have shown promise for SC applications thanks to their distinctive physicochemical properties[4,5]. They differ sharply, however, in how they store charge, how well they conduct, how stable they are, and what practical drawbacks they carry (Table 1). Carbon-based 2D materials rely largely on the EDL; this gives them excellent conductivity and long cycle life, but their capacitance and energy density are intrinsically modest, and they restack badly. Transition-metal oxides and layered hydroxides take the opposite trade-off, delivering high pseudocapacitance yet being held back by poor conductivity, sluggish ion kinetics, and gradual structural breakdown over repeated redox cycling. Insulating materials such as hexagonal BN are electrochemically inactive

© The Author(s) 2026. This is an Open Access article licensed under a Creative Commons Attribution 4.0 International License (https://creativecommons.org/licenses/by/4.0/), which permits unrestricted use, sharing, adaptation, distribution and reproduction in any medium or format, for any purpose, even commercially, as long as you give appropriate credit to the original author(s) and the source, provide a link to the Creative Commons license, and indicate if changes were made.

and serve only as auxiliary or dielectric components. MXenes stand apart in that they pair metallic conductivity (> 7,000 S cm^{-1} for high-quality $Ti_3C_2T_x$) with intercalation pseudocapacitance, which gives high volumetric capacitance while preserving rate capability. Their two main weaknesses, restacking and oxidative degradation, are structural and environmental rather than electrochemical in origin, a distinction that matters, because problems of that kind can be mitigated by compositing with a 3D carbon scaffold. Since the first synthesis of $Ti_3C_2T_x$ in 2011[6], the MXene family, a class of 2D transition-metal carbides, nitrides, and carbonitrides derived from MAX phases, has been widely explored for SC applications[7,8]. As Figure 1 shows, MXene-related publications have risen steeply over the past decade, with energy storage now the leading application area and SCs the largest single focus within it. MXene nanosheets are metallic conductors, providing efficient electron transport pathways[9,10]. In addition, their hydrophilic surfaces and mixed terminations (denoted $-T_x$, such as -O, -OH, and -F) render MXenes accessible to aqueous electrolytes and allow reversible redox reactions between the terminal groups and intercalated cations.

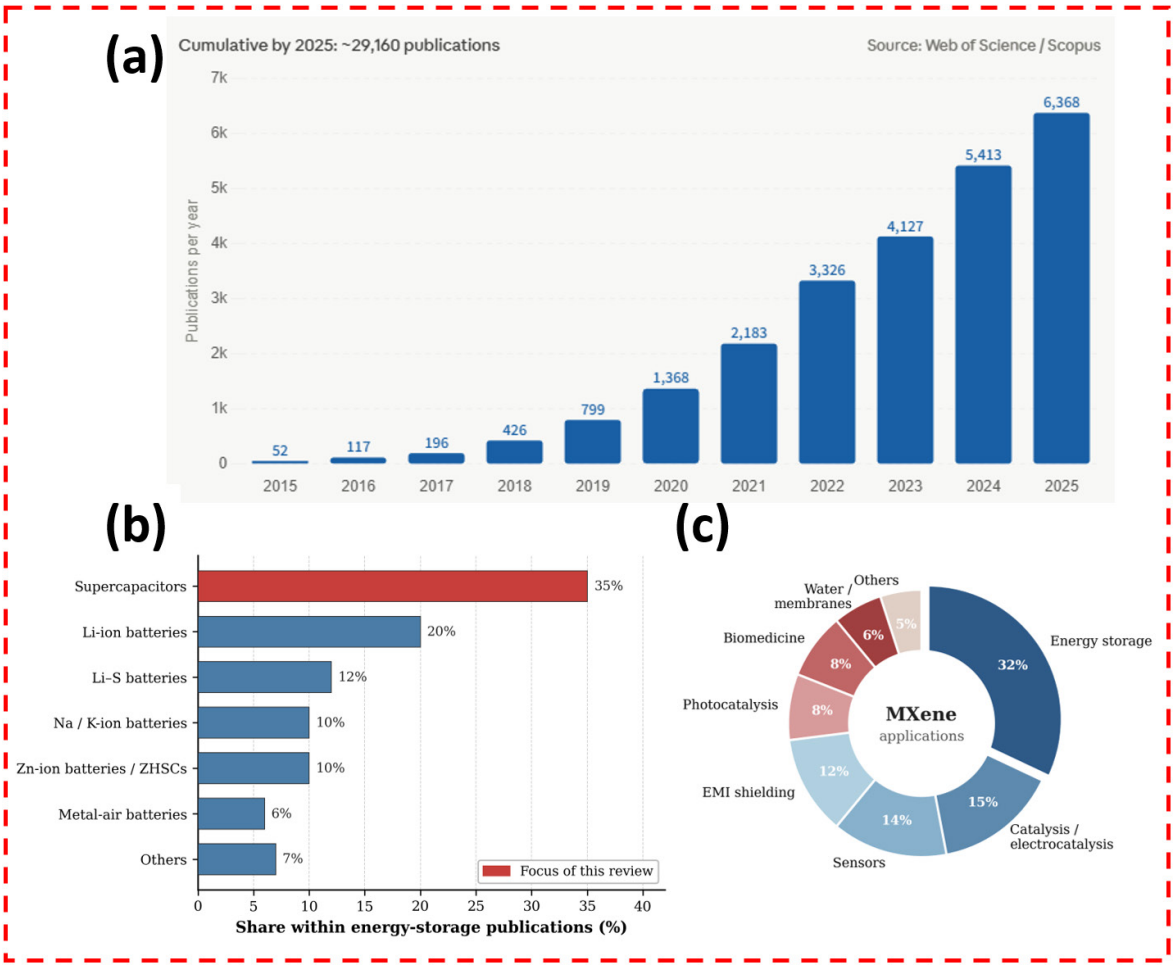


Figure 1. Publication landscape of MXene research and its energy-storage focus (2015-2025). (a) Annual publication output on MXene-related topics from 2015 to 2025; (b) Distribution of MXene research across major application domains; (c) Breakdown of energy-storage device types explored with MXenes, with SCs highlighted as the primary focus of this review. SCs: supercapacitors.

Table 1. Horizontal comparison of representative 2D materials for supercapacitor electrodes.

2D material	Charge-storage characteristic	Electrical conductivity	Structural stability	Practical limitation
Graphene/rGO	EDL-dominated	High	Good	Low capacitance & energy density; restacking reduces active area
Transition-metal oxides/hydroxides	High Pseudocapacitive	Low–moderate (semiconducting)	Moderate; degrades on cycling	Poor conductivity; sluggish kinetics; volume change
Hexagonal BN	Electrochemically inactive	Insulating	High	Inactive; only auxiliary/dielectric use

MXene ($Ti_3C_2T_x$)	EDL and intercalation pseudocapacitance	Metallic (> 7,000 S cm^{-1})	Poor; prone to restacking and oxidation	Restacking and oxidation degrade active area and conductivity

rGO: reduced graphene oxide; EDL: electric double-layer.

Unlike conventional carbon electrodes dominated by the EDL, MXene combines EDL capacitance with intercalation pseudocapacitance, giving high volumetric capacitance (up to ~1,500 F cm^{-3} in H_2SO_4)[11]. However, this dual behavior is not fixed but governed by several coupled factors. In acidic electrolytes, fast reversible proton intercalation coupled to surface redox delivers the highest volumetric capacitance, whereas larger, more strongly hydrated cations in neutral or organic media intercalate less readily, lowering capacitance but widening the voltage window, and viscous ionic liquids extend the window further at the cost of rate. On the MXene side, redox-active -O/-OH terminations and an appropriate amount of confined interlayer water promote pseudocapacitance and proton transport, while inert -F groups block active sites and raise the ion-migration barrier; a wider interlayer spacing lowers ion-transport resistance and exposes more active sites[12].

Importantly, several of these factors can be engineered through the 3D carbon scaffold rather than being left to the intrinsic MXene state: the carbon framework pins the interlayer spacing and suppresses restacking, builds a bicontinuous electron/ion network whose pore hierarchy can be matched to the working ion, and partially shields redox-active terminations from oxidation. The scaffold thus acts not as a passive support but as a structural lever that converts these electrolyte- and surface-dependent factors into stable, device-level performance, motivating the composite designs reviewed in the following sections.

MXenes possess unique 2D layered structures with functionalized surfaces that enable dual energy storage mechanisms, encompassing both EDL capacitance and pseudocapacitance. However, the strong van der Waals forces and hydrogen bonding between adjacent nanosheets render interlayer restacking virtually unavoidable during electrode fabrication and drying processes, which is similar to that of other 2D materials[13,14]. Such restacking significantly reduces accessible active sites, narrows ion-transport channels, and decreases the effective specific surface area, degrading overall energy storage performance. In addition, under ambient conditions, MXenes are prone to oxidation: over time they turn into insulating transition-metal oxides and amorphous carbon. This breaks down the crystal structure and sends the electrical conductivity falling sharply, which in turn cuts into the cycling life and long-term stability of the resulting SCs[15-17].

Addressing these challenges is essential for developing high-performance MXene-based electrodes. Constructing three-dimensional (3D) architectures by integrating MXenes with conductive carbon materials is an effective strategy to suppress restacking and enhance electrochemical performance[18]. While low-dimensional carbons can act as spacers, they often retain lamellar structures with limited ion transport. In contrast, 3D carbon frameworks, such as graphene aerogels, hierarchical porous carbons, carbon nanofiber (CNFs) networks, and biomass-derived carbon foams[19], provide an interconnected skeleton that promotes uniform MXene dispersion, improves ion transport, and enhances structural stability[20-24]. In such composites, the 3D carbon scaffold pins the interlayer spacing to preserve accessible surface area during cycling, provides a bicontinuous electron/ion transport network that shortens ion diffusion pathways, and partially shields MXene surfaces from oxidative environments, thereby extending the operational lifetime of the electrode[25].

The design of MXene/3D-carbon composite electrodes is complicated by multiple tunable variables, including MXene chemistry and surface terminations, carbon precursor and porosity, composite ratio, assembly method, and post-treatment conditions, all of which are strongly coupled and non-linear in their effects on electrochemical performance. Experimental exploration of this design space is time-consuming and difficult to generalize across different systems. Machine learning (ML), which extracts statistical relationships from existing experimental and computational data, has been increasingly adopted as a complementary tool to accelerate the design of MXene/carbon composite SCs[26-30]. Common supervised methods, including random forest (RF), gradient boosting (XGBoost), support vector machines, and artificial neural networks (ANNs), have been used to correlate compositional and structural features with key performance metrics such as specific capacitance, rate capability, and cycling stability. In the design of MXene composites, such models have been used to optimize composition and to predict both electrochemical and mechanical performance. Meanwhile, unsupervised learning and dimensionality-reduction techniques have been used to identify dominant descriptors, such as etching parameters, surface terminations, and active surface area, revealing structure–property correlations that are difficult to capture through traditional empirical screening[31]. In this review, ML is examined not as a standalone topic but as a design-acceleration layer mapped onto the same variables that govern MXene/3D-carbon composites: composition ratio, pore architecture, interlayer spacing, and mechanical response, and we specifically assess how data-driven predictions are coupled back to real synthesis and electrochemical validation in the surveyed studies. Although several reviews on MXene-based SCs have appeared in recent years, they have largely treated either MXene synthesis and general composite strategies or, separately, machine-learning approaches for energy-storage materials in general. To the best of our knowledge, no existing review jointly addresses (i) the rational design of 3D carbon-based MXene architectures, spanning etching, assembly strategies, and the three composite families, and (ii) machine-learning-guided optimization of these same design variables within a single structure–property–design framework. Table 2 summarizes the scope, focus, and limitations of representative recent reviews and positions the present work against them, clarifying its distinct contribution.

Table 2. Comparison of representative recent reviews on MXene-based SCs.

Review	Scope	Main focus	Limitation/gap
Poh *et al.*[32]	MXene synthesis and 3D architecture construction	Etching routes and assembly methods for 3D structures	No ML-guided design; no structure–property–design closed loop
Aravind *et al.*[33]	MXene electrodes broadly, including carbon composites	Etching routes and comprehensive electrode-architecture survey	Descriptive rather than analytical; no unified design logic; no ML
Krishna Paul *et al.*[34]	MXene/cellulose (biomass) composites only	Sustainable biomass-derived composites across 1D/2D/3D forms	Narrow scope (cellulose only); no ML; no pseudocapacitive hybrids
Vattikuti *et al.*[35]	General MXene SC electrodes	ynthesis, characterization, applications, and challenges	No 3D-carbon-specific framework; no ML
This work	3D carbon-based MXene electrodes and ML-guided design	Synthesis, architecture, and ML, in one unified structure–property–design framework	-

SCs: supercapacitors; ML: machine learning.

This review summarizes recent advances in 3D carbon-based MXene composite electrodes for SCs, focusing on synthesis strategies, structural design, and data-driven approaches. Section 2 introduces MXene etching routes and the main methods used to assemble MXene/carbon composites. Section 3 groups existing systems into three types: pure carbon, polymer/biomass-derived, and pseudocapacitive-loaded scaffolds, and compares their performance and limitations. Section 4 covers ML applications in this field, including performance prediction, composition optimization, and mechanical modeling, along with current limitations. Section 5 outlines remaining challenges and future directions, including atomic-level surface engineering, physics-informed ML, and open-access standardized databases. Overall, by connecting rational 3D structural design with data-driven optimization, this review aims to bridge laboratory studies and the practical development of next-generation SCs.

2. Synthesis Strategies

2.1 Etching strategies for MXene synthesis

MXenes are synthesized from MAX-phase precursors ($M_{n+1}AX_n$), in which selective removal of the A-layer leaves M–X slabs capped by surface terminations $-T_x$ (a mixture of -O, -OH, and -F), as shown in Figure 2a. Because the etchant chemistry directly dictates the termination composition, defect density, and oxidation state of the resulting MXene, the choice of etching route is decisive for SC performance. Existing strategies fall into two families: fluorine-containing routes (direct hydrofluoric acid (HF) and *in situ* HF generation) and fluorine-free routes (Lewis-acid molten salt, alkaline/hydrothermal, and electrochemical etching)[36].

2.1.1 Fluorine-containing etching

The earliest and still most widely used routes rely on HF as the active species, introduced either directly or generated *in situ* from a fluoride salt.

Direct HF etching. First reported in 2011 for Ti_3AlC_2 (Figure 2b)[37], this route immerses MAX-phase powder in concentrated aqueous HF at room temperature. The reactions are:

$$Ti_3AlC_2 + 3HF \rightarrow Ti_3C_2 + AlF_3 + (3/2)H_2 \quad (1)$$

$$Ti_3C_2 + 2HF \rightarrow Ti_3C_2F_2 + H_2 \quad (2)$$

$$Ti_3C_2 + 2H_2O \rightarrow Ti_3C_2(OH)_2 + H_2 \quad (3)$$

Here Ti_3C_2 denotes an idealized bare intermediate; the actual product is the heterogeneous mixed-termination $Ti_3C_2T_x$, and each equation is individually balanced. Removal of the rigid Al layer expands the interlayer gap, giving the characteristic accordion-like multilayer morphology held together only by weak van der Waals forces and hydrogen bonds. Despite its high exfoliation efficiency, direct HF etching has two major drawbacks: concentrated HF is highly toxic and corrosive, raising safety concerns at scale; and the high HF activity saturates the basal planes with electrochemically inert -F terminations that suppress pseudocapacitive activity and hinder electrolyte-ion migration.

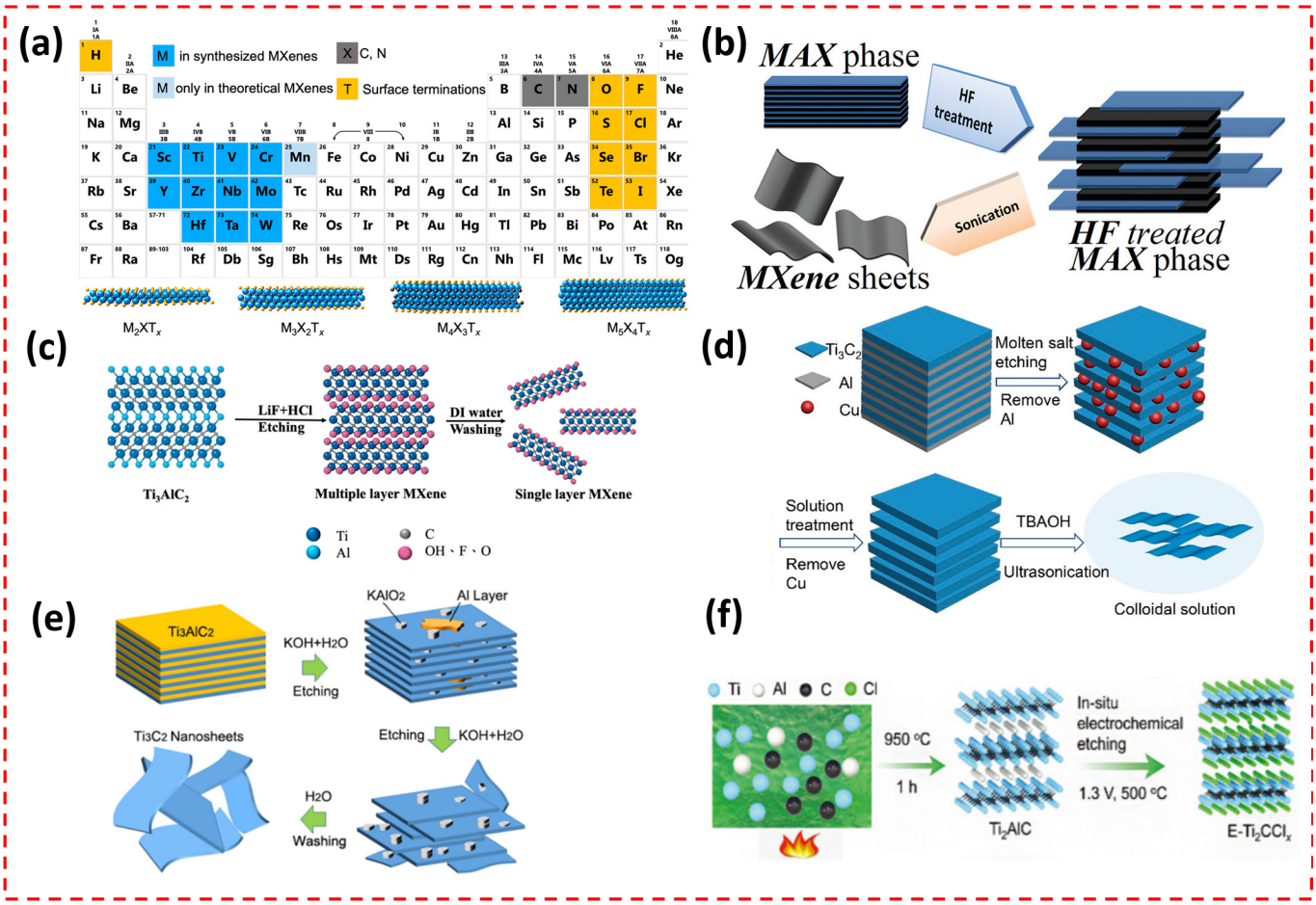


Figure 2. Representative MXene types and etching methods. (a) The types of MXene that have been synthesized. Reproduced from reference[36]. CC BY 4.0; (b) The schematic diagram of MXene is obtained by etching the MAX phase with HF acid. Reproduced with permission from reference[37]. Copyright © 2012 American Chemical Society; (c) HCl/LiF. Reproduced from reference[40]. CC BY 4.0; (d) The synthesis roadmap of MXene was obtained by Lewis-acid molten-salt etching. Reproduced with permission from reference[42]. Copyright © 2021 American Chemical Society; (e) Schematic diagram of Ti_2CT_x obtained by alkaline/hydrothermal etching. Reproduced with permission from reference[44]. Copyright © 2017 American Chemical Society; (f) Schematic diagram of Ti_2CT_x obtained by electrochemical etching of Ti_2AlC. Reproduced from reference[48]. CC BY 4.0. HF: hydrofluoric acid; HCl: hydrochloric acid.

***In situ* HF etching (MILD route).** To mitigate these hazards, the MILD route generates HF *in situ* from a strong acid and a fluoride salt, typically HCl and LiF (Figure 2c)[38-40]:

$$LiF + HCl \rightarrow HF + LiCl \quad (4)$$

HF forms gradually and extracts the Al layer under milder conditions, while Li^+ and water enter the interlayer space as spacers that widen the spacing. The resulting MXenes have fewer -F and more -O groups, and delaminate into stable colloidal suspensions that can be cast into free-standing $Ti_3C_2T_x$ films with conductivity above 1,500 S cm^{-1}. In SCs, the wider interlayer spacing and oxygen-rich terminations together lower ion-transport barriers and expose more active sites, giving faster charge transfer, better cycling stability, and volumetric capacitance up to 900 F cm^{-3} in H_2SO_4. Some residual fluorine nonetheless remains, limiting long-term oxidation stability and motivating fluorine-free methods.

2.1.2 Fluorine-free and green etching routes

To eliminate residual fluorine and gain finer control over surface chemistry, several fluorine-free routes have been developed.

Lewis-acid molten-salt etching. This route replaces aqueous acid with Lewis-acidic molten halide salts at 550-750 °C under an inert atmosphere (Figure 2d). The molten salt converts the Al layer into volatile chlorides, introducing highly crystalline, fluorine-free -Cl and -O terminations[41,42]; the resulting MXenes show enhanced pseudocapacitive activity in mild aqueous electrolytes and extend the voltage window of asymmetric SCs relative to HF-etched counterparts.

Alkaline/hydrothermal etching. Exploiting the amphoteric nature of A-layer elements such as Al, this route uses concentrated alkali

under elevated temperature and pressure to dissolve the A-layer (Figure 2e). Base concentration and temperature must be controlled to avoid premature precipitation of metal hydroxides that can jam the reaction[43-46]. It yields MXenes functionalized exclusively with electroactive -OH and -O terminations, free of fluorine.

Electrochemical etching. Here the MAX phase serves as the anode in a mild chloride electrolyte such as dilute HCl (Figure 2f); under an appropriate anodic potential, the Al layer is selectively removed by electrochemical corrosion near ambient temperature[47-49]. The applied potential allows control over the etching process and surface terminations, producing fluorine-free flakes with high intrinsic conductivity.

In summary, fluorine-containing routes operate under milder conditions and at lower cost but leave residual fluorine that limits long-term stability, whereas the molten-salt, alkaline-hydrothermal, and electrochemical routes eliminate fluorine, boosting pseudocapacitive activity, at the expense of higher temperatures, specialized atmospheres, or precise electrochemical control. The choice of route therefore balances process simplicity against surface-chemistry quality and stability.

2.2 Assembly strategies for MXene/carbon composite electrodes

Once MXene nanosheets have been exfoliated, the way in which they are combined with carbonaceous components determines the resulting composite's pore architecture, interfacial contact, and mechanical integrity, all of which strongly influence the final electrochemical response. Three strategies dominate the current literature: solution-based mixing and self-assembly, *in situ* growth and carbonization, and template-assisted assembly.

2.2.1 Solution-based mixing and self-assembly

Solution-based mixing and self-assembly are one of the most straightforward and widely adopted strategies for constructing MXene/carbon composites[50-52]. As shown in **Figure3**a, it exploits the hydrophilicity and colloidal dispersibility of delaminated $Ti_3C_2T_x$ nanosheets in aqueous and polar media, which allow direct mixing with carbon components such as carbon nanotubes (CNTs), graphene (or reduced graphene oxide, rGO), and carbon quantum dots. Assembly is driven by non-covalent interactions, including electrostatic attraction, van der Waals forces, and hydrogen bonding between the oxygen-containing surface groups of the two components, which stabilize the hybrid dispersion and promote a uniform network. Once introduced, the carbon phase serves as a physical spacer that suppresses the face-to-face self-restacking of MXene layers, helping to preserve the accessible surface area and the ion-transport pathways under repeated cycling.

Depending on the post-processing step, this strategy allows the composite morphology to be tuned between two limiting forms. Vacuum-assisted filtration yields flexible, free-standing films with well-defined lamellar structures, whereas directional freeze-drying (ice templating) produces interconnected 3D aerogels characterized by high specific surface area, short ion-diffusion pathways, and better tolerance to electrode swelling during cycling. The main advantages of solution-based assembly are its scalability, low cost, and preservation of the intrinsic electronic conductivity of each component; its main drawback is that the composite is held together almost entirely by non-covalent forces, so interfacial cohesion and long-term mechanical stability under high-stress cycling are often limited.

2.2.2 *In situ* growth and carbonization

To address the weak interfacial adhesion of physically assembled composites, *in situ* growth and carbonization have emerged as a more robust route for constructing MXene/carbon heterostructures. In this approach, a carbon precursor, such as dopamine, glucose, or a polymerizable monomer, is first deposited onto the surface of delaminated $Ti_3C_2T_x$ nanosheets via a hydrothermal or solvothermal step, and is then converted to a carbon shell by controlled high-temperature carbonization, as shown in Figure 3b[53]. Because the carbon phase nucleates and grows directly on the MXene template, the resulting interfacial contact is stronger and more uniform than in solution-mixed systems.

This approach also improves the mechanical strength and heat resistance of the composite, and the carbon layer helps protect MXene from oxidation during long cycling. When nitrogen containing precursors such as dopamine are used, the carbon layer is doped with nitrogen, adding more active sites and improving ion transport. The resulting core–shell or interconnected structures have wider interlayer spacing and better electrochemical durability, making them well suited for SC electrodes that need both high rate capability and long cycle life.

2.2.3 Template-assisted assembly

Template-assisted assembly enables precise control over the 3D architecture of MXene/carbon composites. It relies on preformed sacrificial frameworks, such as polymer spheres, metal–organic frameworks (MOFs), or ice crystals, to spatially organize MXene and carbon precursors.

MXene and a carbon precursor are deposited on or within a sacrificial template, which is subsequently removed by thermal decomposition or chemical etching[54,55]. This process leaves a porous structure whose pore size, shape, and connectivity are

determined by the template, as shown in Figure 3c. Among various approaches, ice templating is widely used to fabricate 3D carbon/MXene aerogels. During freezing, ice crystals grow directionally and are subsequently removed by sublimation, forming aligned lamellar channels that facilitate ion transport and enhance mechanical stability.

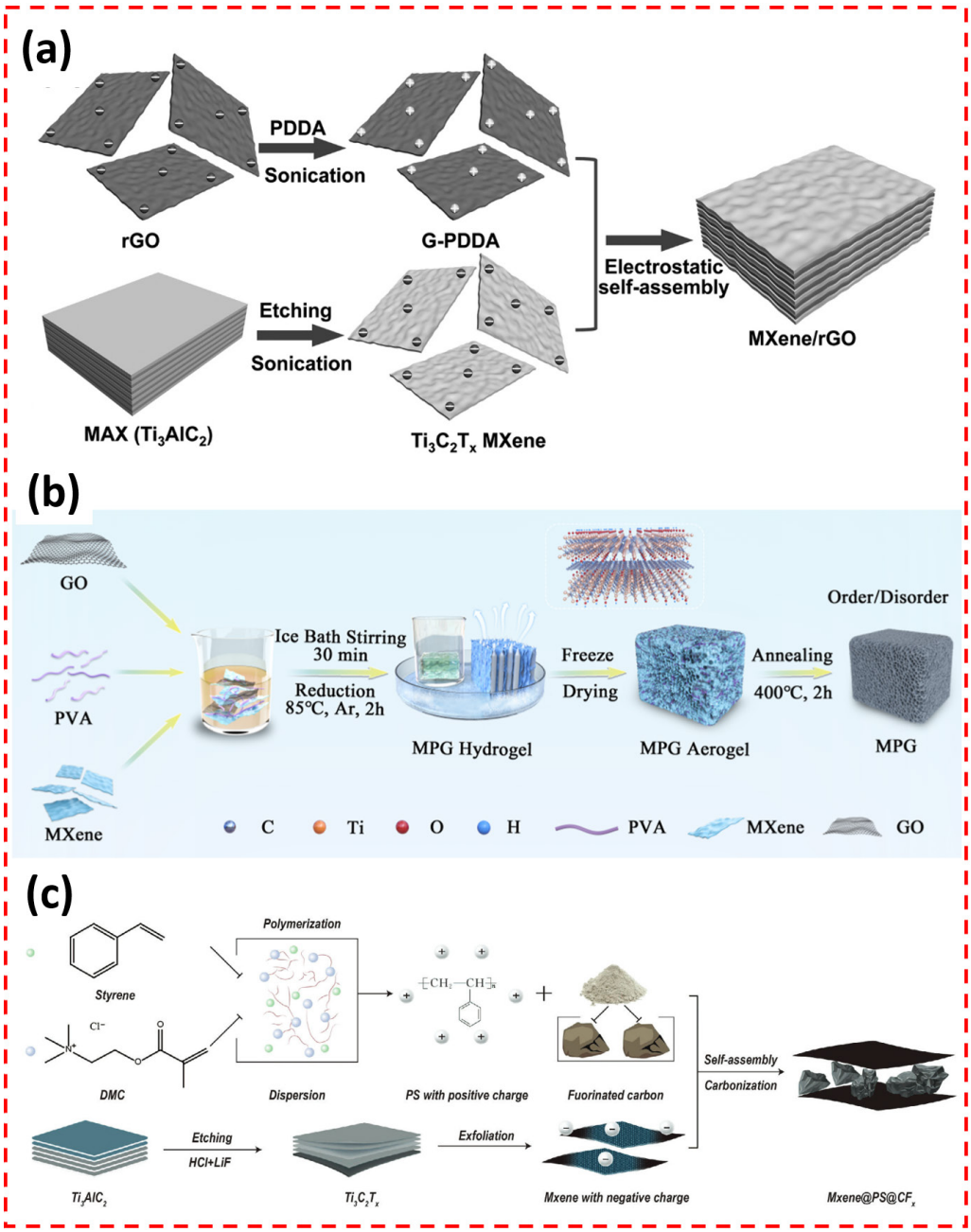


Figure 3. Schematic illustration of the three assembly strategies used to construct 3D MXene/carbon composite electrodes. (a) Solution-based mixing and self-assembly, in which exfoliated MXene nanosheets and carbon components co-assemble in aqueous dispersion through non-covalent interactions to form a 3D porous network. Reproduced with permission from reference[52]. Copyright © 2017 John Wiley & Sons; (b) *In situ* growth and carbonization, in which a carbon precursor is grown on the MXene template and subsequently carbonized into a conductive 3D scaffold. Reproduced with permission from reference[53]. Copyright © 2025 American Chemical Society; (c) Template-assisted assembly, in which a sacrificial or structural template directs the formation of an ordered, anisotropic pore architecture. Reproduced with permission from reference[55]. Copyright © 2025 John Wiley & Sons. rGO: reduced graphene oxide; PVA: polyvinyl alcohol; PS: polystyrene; CF: carbon framework.

The main advantage of template-assisted assembly lies in its ability to precisely control pore size distribution, structural anisotropy, and mass transport pathways, thereby improving electrolyte accessibility and electrochemical kinetics. The main drawback is that the use of sacrificial templates introduces additional processing steps and cost, which limits scalability. Despite this, template-assisted routes remain important when the target electrode requires a well-defined 3D architecture tailored to a specific performance requirement.

To clarify the relative advantages of composites prepared by different strategies, Table 3 compares the three assembly routes across interfacial bonding, pore control, conductivity, mechanical stability, scalability, and the best-suited application scenario. Solution-based self-assembly best preserves intrinsic conductivity and offers the highest scalability, making it preferred for high-throughput fabrication of flexible films and aerogels when cost and processability are the primary constraints; its non-covalent interfaces, however, limit mechanical durability under high-stress cycling. *In situ* growth and carbonization yield the strongest interfaces and best oxidation resistance and are therefore favored when interfacial cohesion and heteroatom doping are critical, at the expense of an energy-intensive high-temperature step that can partially sacrifice pseudocapacitive -O/-OH terminations. Template-assisted assembly provides the most precise control over pore architecture and ion-transport anisotropy, and is reserved for electrodes whose performance depends on a pre-determined 3D architecture, though the use of sacrificial templates raises cost and limits scalability. Overall, no single strategy is universally optimal: the choice is dictated by whether conductivity/cost, interfacial robustness, or architectural precision is the dominant priority.

Table 3. Comparison of the three assembly strategies for MXene/carbon composite electrodes.

Strategy	Interfacial bonding	Pore/structure control	Conductivity preservation	Mechanical stability	Scalability & cost	Best-suited scenario
Solution-based mixing and self-assembly	Weak	Moderate	High	Limited under high-stress cycling	High; water-based, low cost	Flexible films/aerogels; high-throughput, cost-sensitive fabrication
In situ growth and carbonization	Strong	Moderate	Reduced if -O/-OH lost at high *T*; recoverable via heteroatom (N) doping	Improved strength, heat resistance, oxidation protection	Lower; energy-intensive high-*T* step	Long-term oxidation resistance, strong interfaces, heteroatom doping
Template-assisted assembly	Defined by template; generally moderate–strong	Precise	High	Good	Low; extra steps, sacrificial-template cost	Electrodes needing a well-defined 3D architecture or anisotropic ion transport

3. Research Progress on 3D MXene/Carbon Composite Systems

To compare the three composite types on a common basis, we examine each from several angles: structure, charge-storage behavior, electrochemical performance, mechanical robustness, cycling stability, and practical feasibility. Particular attention is given to the 3D framework and the MXene–carbon interfaces, to the relative contributions of EDL capacitance and pseudocapacitance, and to the trade-offs among synthesis complexity, cost, and scalability.

The three categories, conductive nanocarbon, polymer/biomass-derived carbon, and pseudocapacitive additives, are distinguished by the dominant role of the non-MXene component. Conductive nanocarbons mainly build a highly conductive network and add EDL capacitance. Polymer- and biomass-derived carbons act chiefly as structural frameworks, reinforcing mechanical integrity and preserving porous architectures, with the capacitance developed on carbonization playing a secondary part. Pseudocapacitive additives are introduced to raise energy density through extra redox reactions.

These roles are not mutually exclusive, and a single architecture often contains more than one. Because pseudocapacitive components are usually carried on a conductive or structural carbon framework, some compositional overlap between categories is inevitable. The classification therefore follows the dominant charge-storage mechanism and the overall design intent rather than the mere presence of a given constituent. A Co_3O_4/MXene/rGO electrode, for example, includes an rGO conductive network yet is grouped with the pseudocapacitive composites, since the Faradaic contribution of Co_3O_4 governs both its electrochemical behavior and its design objective.

The benefits of 3D architectures are most clearly understood by mapping each structural parameter onto a measurable electrochemical signature rather than onto final capacitance alone. First, conductive-network continuity governs the charge-transfer resistance (R_ct). A bicontinuous MXene–carbon network provides uninterrupted electron pathways, manifested as a smaller semicircle in the high-frequency region of the Nyquist plot (lower R_ct), whereas discontinuous or weakly bonded networks enlarge this semicircle and raise polarization. Second, pore-size distribution and interlayer spacing control the ion-diffusion impedance and rate performance. Hierarchical macro-/meso-/micropores together with widened interlayer spacing shorten ion-diffusion paths, producing a more vertical low-frequency Warburg line (lower diffusion impedance) and flatter capacitance-retention curves at high

current densities; narrow or restacked channels steepen the Warburg slope toward 45° and cause rapid capacitance fade with increasing rate. Third, the charge-storage mechanism dictates the cyclic voltammetry (CV) shape and galvanostatic charge–discharge (GCD) profile. EDL-dominated carbon networks give near-rectangular CV curves and linear, symmetric GCD profiles, whereas pseudocapacitive loading (metal compounds, -O/-OH redox) introduces broad redox humps in CV and quasi-plateaus or non-linear regions in GCD, so the degree of distortion reflects the EDL-to-pseudocapacitance balance set by the 3D design. Finally, interface bonding determines how these signatures evolve on cycling: strong covalent or molecular-bridged interfaces keep *R*_ct and the CV/GCD shape stable over thousands of cycles, while weak non-covalent contacts progressively enlarge *R*_ct and shrink the CV area, appearing as accelerated capacitance decay.

3.1 Composites of MXenes and carbon nanomaterials

Early work on MXene/carbon-nanomaterial composites focused primarily on the construction of 3D skeletons and the optimization of their mechanical stability. Shao *et al.*[50] used ascorbic acid to induce self-assembly at room temperature, thereby avoiding the pore-defect formation typically observed during high-temperature hydrothermal processing; the resulting MXene/rGO aerogel exhibited a yield stress of 16.18 MPa and was robust enough to support a 500 mL water container without deformation, while as a self-supported electrode it delivered a specific capacitance of 233 F g^{-1} with ~91% retention after 10,000 cycles. Building on this foundation, Wang *et al.*[56] used a similar MXene/rGO aerogel in a zinc-ion hybrid SC that retained over 95% of its initial capacitance after 75,000 cycles at 5 A g^{-1}, as shown in Figure 4a, confirming that MXene/carbon 3D scaffolds give excellent long-term cycling stability. However, ascorbic acid reduction at room temperature leaves residual oxygen groups that limit conductivity; the narrow voltage window of aqueous electrolytes (~1.0–1.6 V) constrains energy density; and zinc dendrite growth introduces safety risks.

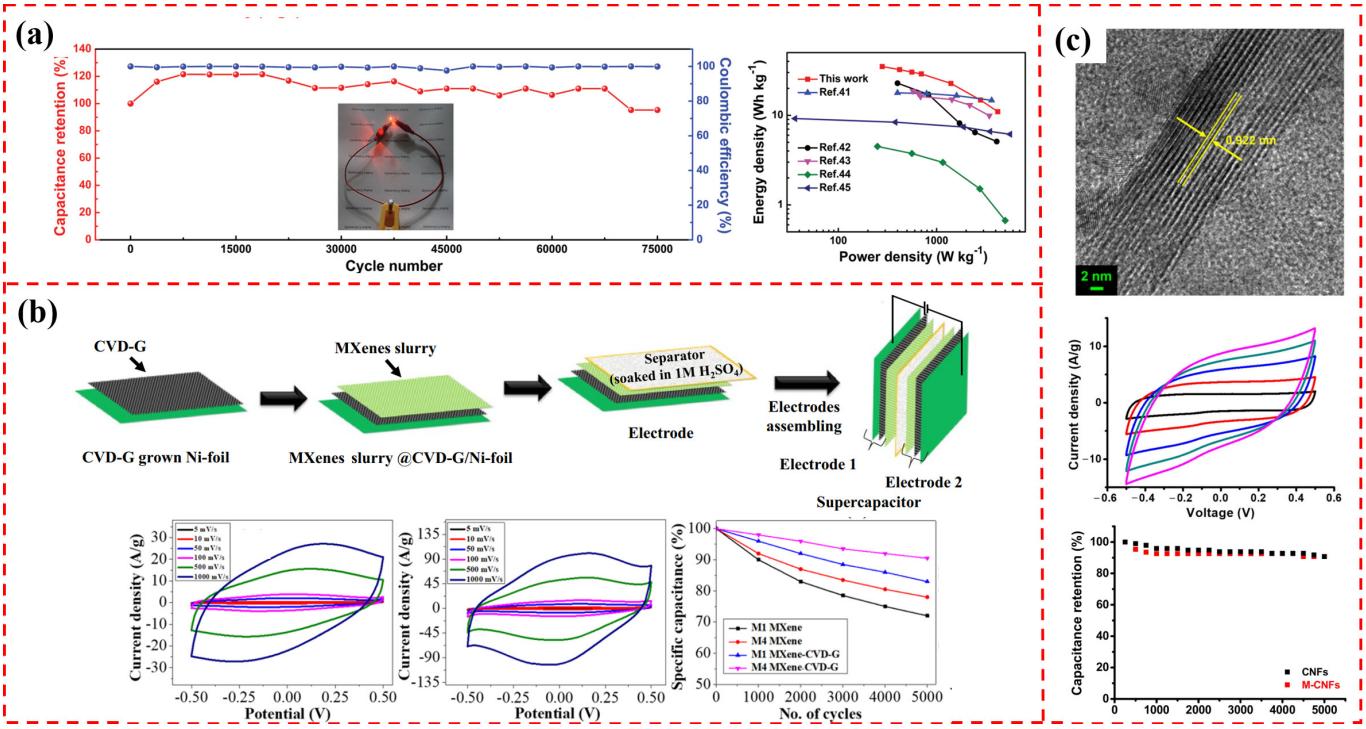


Figure 4. Representative MXene/carbon-nanomaterial 3D scaffolds and their electrochemical performance. (a) MXene/rGO zinc-ion hybrid SC retaining over 95% of its initial capacitance after 75,000 cycles at 5 A g^{-1}. Reproduced with permission from reference[56]. Copyright © 2019 John Wiley & Sons; (b) $Ti_3C_2T_x$/graphene/Ni electrode: (i) fabrication process; (ii) CV curves (M1, M4); (iii) cycling stability over 5,000 cycles. Reproduced from reference[59]. CC BY 4.0; (c) M-CNF electrode: (i) HR-TEM image; (ii) CV curves; (iii) cycling stability. Reproduced from reference[60]. CC BY 4.0. rGO: reduced graphene oxide; SC: supercapacitor; CV: cyclic voltammetry; M-CNF: MXene-coated carbon nanofibers; HR: high-resolution; TEM: transmission electron microscopy.

To enrich the 3D pore architecture and extend the storage mechanism, subsequent studies sought improvements along two complementary axes: structural morphology and chemical modification. Xu *et al.*[57] interwove one-dimensional CNTs with 2D MXene nanosheets to construct a composite aerogel with more uniform porosity; the more continuous conductive network and hierarchical pores lower the charge-transfer and ion-diffusion impedance, so that the resulting flexible device exhibited near-rectangular CV curves with negligible electrochemical decay under different bending angles. Liu *et al.*[58] introduced S and N heteroatoms into an rGO network, which simultaneously improved electrode wettability, reflected in a steeper, more vertical low-frequency Warburg line and reduced diffusion impedance, and provided additional Faradaic reaction sites that appear as broad redox humps superimposed on the otherwise rectangular CV background; the all-solid-state symmetric device retained nearly 100% of its capacity after 10,000 cycles,

with the energy density increased to 24.2 Wh kg^{-1} and a slow self-discharge profile that allowed a series-connected stack to power an LED. However, the interaction between CNTs and MXene lacks strong chemical bonding, so under high-frequency compressive fatigue the interfacial cohesion remains a potential source of structural failure; heteroatom doping, usually completed at the precursor stage, is also difficult to render uniform throughout a macroscopic aerogel interior.

Beyond porosity and heteroatom doping, both the conductive network and the carbon–MXene interface can be engineered to lower resistance and improve ion access. Kumar *et al.*[59] showed that engineering the carbon–current-collector interface is critical: by passivating the Ni current collector with CVD-grown graphene to form a $Ti_3C_2T_x$/graphene/Ni electrode (Figure 4b), they raised the specific capacitance to 542 F g^{-1} at 5 mV s^{-1}, more than 1.5 times that of the graphene-free device, while preserving a quasi-rectangular CV shape and symmetric GCD profile over 5,000 cycles, confirming that interfacial engineering of the conductive pathway, not only the active material, governs the EDL response. Adopting a complementary scaffold strategy, Kim *et al.*[60] dip-coated electrospun carbon CNFs into a Ti_3C_2 colloidal solution to build a free-standing MXene-coated CNF electrode (Figure 4c); benefiting from the pseudocapacitive contribution of the MXene coating on the porous, conductive CNF backbone, this binder-free electrode delivered a specific capacitance of 514 F g^{-1} at 0.5 A g^{-1} with an energy density of 71.4 Wh kg^{-1} and 90.7% retention after 5,000 cycles in 1 M Na_2SO_4, while the CNF network shortens ion-transport pathways and suppresses MXene restacking.

To address the detrimental effect of MXene surface terminations on electrochemical performance, several studies have targeted the etching chemistry and post-treatment steps. Ren *et al.*[61] prepared fluorine-free MXene via a Lewis-acid ($ZnCl_2$) molten-salt route, which eliminated the electrochemically inert –F terminations introduced by conventional HF etching and instead exposed the more storage-active –O and –Cl groups; when composited with rGO, the more redox-active surface enhances the pseudocapacitive contribution in CV, and the electrode retained 100% of its capacity over 20,000 cycles. Zhao *et al.*[62] introduced a different approach: Zn^{2+}-induced gelation followed by ultraviolet (UV) photothermal treatment, which simultaneously achieved *in situ* nitrogen doping and defluorination, conferring room-temperature oxidation stability and a record volumetric capacitance of 1,323 F cm^{-3} that surpassed previously reported MXene-based devices on the Ragone plot. Each route, however, entails its own processing limitation: molten-salt etching requires 550–750 °C under an inert atmosphere, raising the cost of scale-up, while UV penetration is intrinsically limited, so for 3D aerogels of non-trivial thickness the degree of doping and defluorination varies between the surface and the interior core, undermining electrode uniformity.

Assessed against the six criteria, this category occupies a clear niche. In structural design and mechanism, the carbon skeleton stores charge mainly through the EDL with no high-capacity Faradaic component, so device-level energy density is inherently capped. Structurally, MXene and carbon are joined mainly by weak non-covalent forces, giving poor interfacial adhesion that makes the 3D network prone to collapse under repeated stress and limiting mechanical robustness, especially for flexible devices. Its decisive strengths lie in cycle life and feasibility: these systems are simple and low-cost to fabricate and set the benchmark for stability, consistently retaining over 90% of their capacitance across 10,000–75,000 cycles.

3.2 Composites of MXenes with polymer- and biomass-derived scaffolds

Biomass scaffolds offer an effective route to reconcile mechanical deformability with stable charge storage. Jiao *et al.*[63] prepared freestanding MXene/bacterial-cellulose (BC) composite paper through an all-solution paper-making process, then applied laser-cutting kirigami patterning to construct stretchable all-solid-state micro-supercapacitor arrays (Figure 5a). By modulating the interlayer spacing and exploiting the hydrogen-bonded BC network, the electrode achieved an areal capacitance of 111.5 mF cm^{-2} while remaining stable under 100% stretching and in bent or twisted states, demonstrating that a biomass scaffold can simultaneously deliver structural deformability and stable areal performance. The insulating cellulose matrix, however, contributes no charge storage of its own and can dilute the volumetric capacitance if its loading is too high. Wang *et al.*[64] introduced polydopamine (PDA) as a molecular bridge to connect MXene with graphene networks; the strong molecular-bridged interface improved compressive strength and mechanical stability and helped maintain a stable *R_ct* on cycling, enabling applications in both energy storage and pressure sensing. The polymerization of PDA is slow and pH-sensitive, which complicates processing and limits large-scale fabrication.

In some research, polymers serve not only as structural supports but also as carbon precursors. Lu *et al.*[65] combined $Ti_3C_2T_x$ nanosheets with polyvinyl alcohol (PVA) through hydrogen bonding. Directional freeze-drying using liquid nitrogen produced an ordered porous structure, while subsequent heating at 400 °C under an argon atmosphere converted PVA into amorphous carbon. This process expanded the $Ti_3C_2T_x$ interlayer spacing and introduced microporous defects, increasing the number of accessible active sites; the expanded interlayer spacing and added micropores also lower the ion-diffusion impedance, which is reflected in retained rate capability rather than capacitance alone. The best electrode (MPA2.0, $Ti_3C_2T_x$: PVA = 1:2 by mass) gave 348.14 F g^{-1} at 2 mV s^{-1}, and the corresponding symmetric SC delivered 37.8 Wh kg^{-1} at 1,800 W kg^{-1}, stabilizing at 92.52% retention after 10,000 cycles at 10 A g^{-1}. However, high-temperature treatment is energy-intensive and destroys the –O and –OH groups responsible for MXene pseudocapacitance, reducing active sites. A complementary, carbonization-free strategy combines a biomass binder with a conductive polymer: Xu *et al.*[66] linked MXene nanosheets with CNFs and polyaniline (PANI) into a flexible aerogel film (Figure 5b), in which the hydrogen-bonded CNF network raised the mechanical strength of MXene from 44.25 to 119.56 MPa while the PANI

conductive template delivered a specific capacitance of 327 F g^{-1} with a low resistance of 0.23 Ω, retaining 71.6% of its capacitance after 3,000 cycles and 500 folding cycles, showing that polymer/biomass dual modification can reconcile flexibility with charge storage without an energy-intensive carbonization step. Chen *et al.*[67] took a different approach by using the natural channels of balsa wood as a pre-existing 3D skeleton. An all-wood electrode was fabricated via vacuum-assisted drop casting combined with Ni^{2+}-induced Ti_3C_2 cross-linking, without carbonization. As shown in Figure 5c, scanning electron microscopy and energy-dispersive X-ray spectroscopy confirm that the Ti_3C_2 aerogel uniformly fills the wood vessel pores, forming a conductive 3D network for electron and ion transport. The electrode achieved a conductivity of 323.6 S m^{-1} and an areal capacitance of 930 mF cm^{-2} at 0.5 mA cm^{-2}, retaining 88.2% at 10 mA cm^{-2}, much better than the Ni^{2+}-free control. The macropores of wood act as electrolyte reservoirs while aerogel-type mesopores shorten local diffusion paths, giving low ion-diffusion impedance and the strong rate retention observed at high current density. However, the insulating lignin and cellulose matrix means that electrical conduction relies on the surface MXene coating, which can limit performance at high mass loadings.

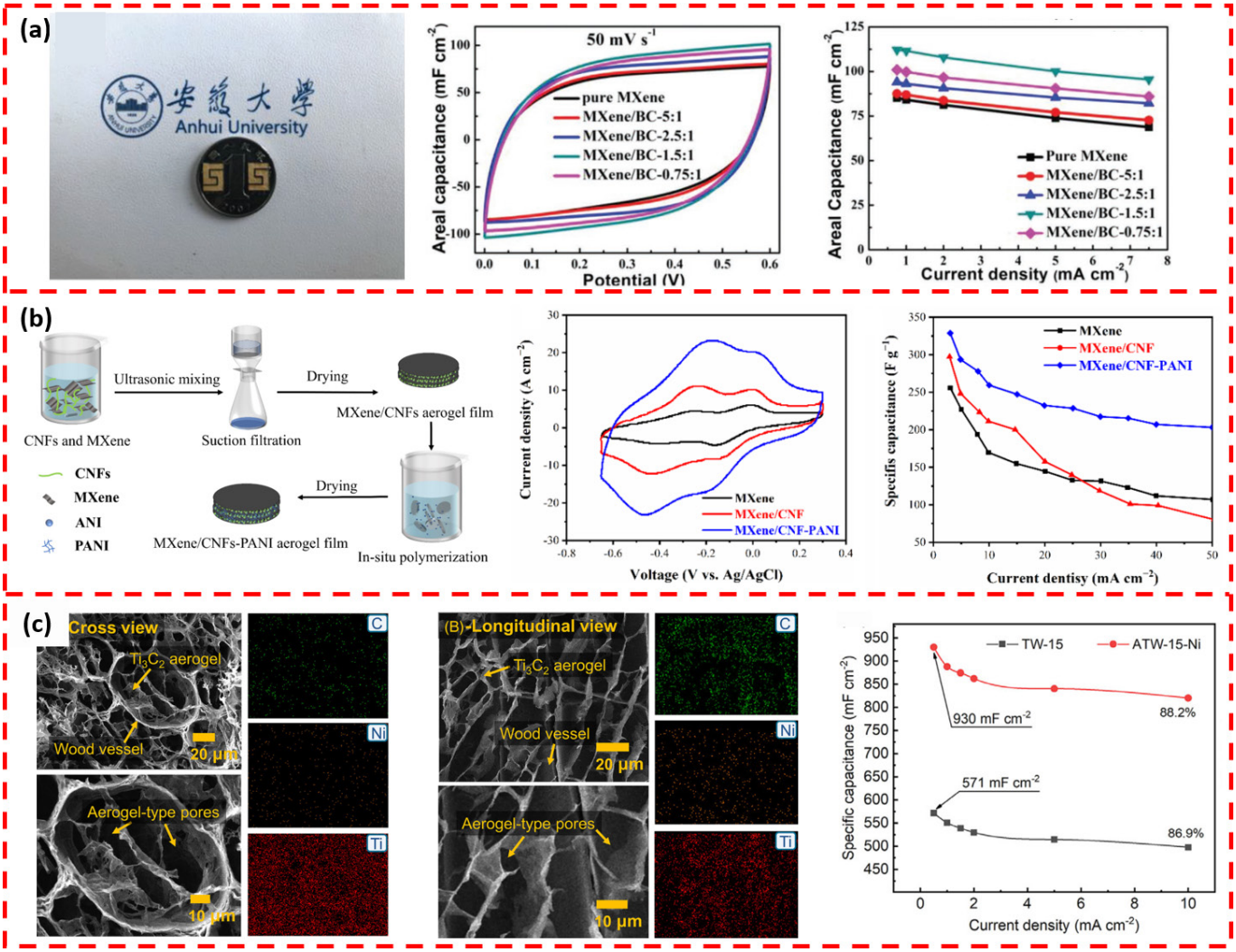


Figure 5. Representative MXene composites with polymer- and biomass-derived 3D scaffolds. (a) MXene/BC kirigami micro-supercapacitor array: (i) device photograph; (ii) CV curves at 50 mV s^{-1}; (iii) areal capacitance versus current density, delivering 111.5 mF cm^{-2} with stability up to 100% strain. Reproduced from reference[63]. CC BY 4.0; (b) Nanocellulose-linked MXene/CNF-PANI aerogel film: (i) preparation scheme; (ii) CV curves; (iii) specific-capacitance comparison, reaching 327 F g^{-1} with mechanical strength up to 119.56 MPa. Reproduced from reference[66]. CC BY 4.0; (c) Structural characterization confirming uniform Ti_3C_2 aerogel infilling within natural wood vessel pores, giving an all-wood electrode with high rate capability and an areal capacitance of 930 mF cm^{-2}. Reproduced from reference[67]. CC BY 4.0. BC: bacterial-cellulose; CV: cyclic voltammetry; CNF: carbon nanofibers; PANI: polyaniline.

Within the same six-criterion comparison, this category stands out for its structural and mechanical integrity, though that strength comes with real trade-offs. The underlying difficulty is that conductivity and mechanical reinforcement pull in opposite directions: biomass and polymers are insulating, so recovering MXene's metallic conductivity requires high-temperature treatment, and that same treatment strips away the -O/-OH groups that supply pseudocapacitance, which places a ceiling on achievable performance. The fibrous, cross-linked networks do pay off in stability and cycle life; the PVA-derived system, for instance, retains 92.52% of its

capacitance over 10,000 cycles. The real limitation is feasibility: dopamine polymerization and freeze-pyrolysis are time- and energy-intensive, which makes scale-up considerably harder than for pure-carbon systems.

3.3 Composites of MXenes with pseudocapacitive nanomaterials

In the two categories above, pure-carbon skeletons provide excellent conductivity and cycling stability but remain subject to the EDL-capped ceiling on energy density, and polymer-/biomass-reinforced systems, although mechanically improved, still yield only modest gains in capacitance. To raise the energy-density ceiling, a third group of studies has built on the 3D MXene/carbon framework by introducing transition-metal compounds, layered double hydroxides (LDHs), or MOF derivatives, all of which have very high theoretical capacities, so that EDL and pseudocapacitive contributions act in a complementary manner.

Liu *et al.*[68] embedded Co_3O_4 nanoparticles into an MXene/rGO 3D network through an *in situ* reduction followed by thermal annealing; the resulting CMR31 composite delivered 345 F g^{-1} at 1 A g^{-1} with a charge-transfer resistance of only 0.44 Ω. This small R_t reflects the continuous MXene/rGO electron network that minimizes interfacial charge transfer, consistent with the rectangular-to-redox CV transition expected from EDL–pseudocapacitive coupling, and the assembled all-solid-state asymmetric device, when connected in series, was able to power an LED. However, the binding between the metal oxide and the carbon substrate relies on physical adsorption or *in situ* growth, so partial dissolution of metal ions and interfacial detachment remain risks under prolonged cycling or high-rate operation. To reduce the cost of the 3D scaffold, Liao *et al.*[69] replaced graphene aerogel with melamine-derived N-doped carbon foam as the support and grew CoS *in situ* to provide Faradaic capacity; as illustrated in Figure 6a, the synthesis route condenses etching, immersion, and one-step annealing into a compact workflow, and the resulting electrode delivered 250 F g^{-1} at 1 A g^{-1} while retaining 97.5% of its capacity after 10,000 cycles (Figure 6b). The dominantly macroporous structure of melamine-derived carbon foam, however, offers a much smaller specific surface area than graphene aerogel, which limits further increases in volumetric capacitance.

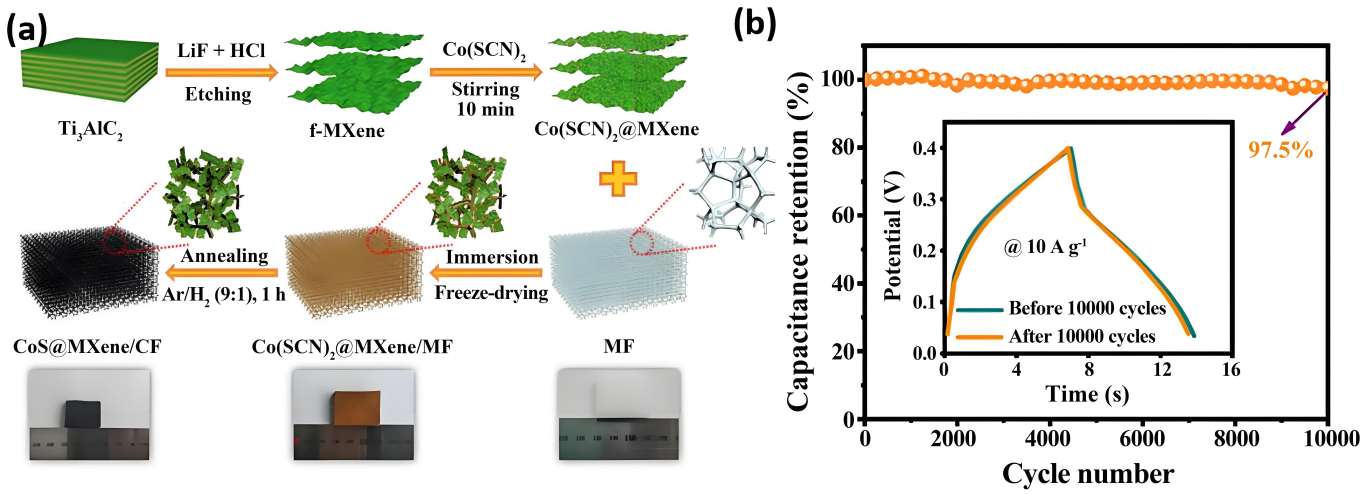


Figure 6. CoS@MXene/melamine-derived N-doped carbon-foam aerogel. (a) One-pot synthesis route; (B) Cycling stability, retaining 97.5% capacitance over 10,000 cycles. Reproduced with permission from reference[69]. Copyright © 2021 American Chemical Society. HCl: hydrochloric acid; MF: melamine foam.

To address the fatigue failure associated with the pronounced volume change of battery-type metal compounds during charge/discharge, Zhang *et al.*[70] converted NiCo-LDH into $NiCo_2O_4$ and anchored the product onto an MXene/rGO skeleton; the 3D carbon network effectively buffers the local stress, so that the assembled compressible device sustains stable capacitance retention across compressive strains from 0% to 60% and across 100 compress-release cycles at 50% strain, reconciling high compressive tolerance with high energy storage. Nonetheless, the intrinsic reaction kinetics of battery-type materials such as $NiCo_2O_4$ remain limited by sluggish bulk ion diffusion at very high rates, which manifests as a steeper low-frequency Warburg slope and pronounced polarization in GCD, leading to reduced rate capability. Building on this direction, Xu *et al.*[71] turned to MOF derivatives with high theoretical capacity: using sodium carboxymethyl cellulose as a flexible carbon-precursor scaffold and MXene as a conductive dispersant, they co-gelated the components *in situ* and pyrolysed ZIF-67, a stress-accommodation design in which the soft carbon matrix buffers the volume expansion of the rigid MOF-derived particles. This design suppresses pulverisation during cycling and delivers 48.4 Wh kg^{-1} at a power density of 699.8 W kg^{-1}, outperforming a series of recently reported Co-based ASCs. The preparation of MOF precursors and the multistep pyrolysis, however, are time-consuming and poorly compatible with low-cost scale-up. In a different direction, Jing *et al.*[72] used a molybdate-assisted hydrothermal reaction to partially and reversibly oxidise the MXene surface, constructing a 3D heterostructured aerogel of mixed-valent metals; combined with a wide-voltage ternary ionic-liquid electrolyte, this design activates high-voltage pseudocapacitance from an electrolyte-window perspective, achieving a 2.6 V stable window and an energy density of 28.3 Wh kg^{-1} at 1,193 W kg^{-1}. In CV, this widened 2.6 V window manifests as an extended potential

range free of electrolyte-decomposition current spikes, while the mixed-valent redox appears as broad humps superimposed on a capacitive background. Partial oxidation of MXene, however, inevitably sacrifices part of the metallic carbide core, and the high room-temperature viscosity of ionic-liquid electrolytes negatively affects the response at very high rates.

According to the six evaluation criteria, pseudocapacitive composites offer the highest device-level energy density, albeit at the expense of cycling stability and practical applicability. During ion insertion and extraction, transition-metal compounds undergo repeated phase transformation and volume change. This tends to agglomerate and pulverize the particles, which gradually lose contact with the conductive framework, so cycling durability falls below that of carbon-based systems. Their intrinsically low electrical conductivity is a second drawback: it slows charge transport and produces pronounced polarization at high rates, which holds back rate performance. Synthesis is a further constraint. It often runs through several steps: precursor preparation, *in situ* hydrothermal growth, high-temperature sulfidation, or MOF-derived pyrolysis, each sensitive to reaction conditions, which makes reproducibility, scale-up, and cost control difficult.

Comparison of the three composite types highlights the inherent trade-offs among electrochemical performance, structural stability, and practical feasibility, as summarized in Table 4 and Figure 7. The practical implication is less that one type is best than that each suits a different priority: pseudocapacitive composites where energy density is the leading requirement, carbon-dominated ones where cycle life and manufacturability matter most, and polymer/biomass-derived frameworks in between when mechanical robustness is decisive.

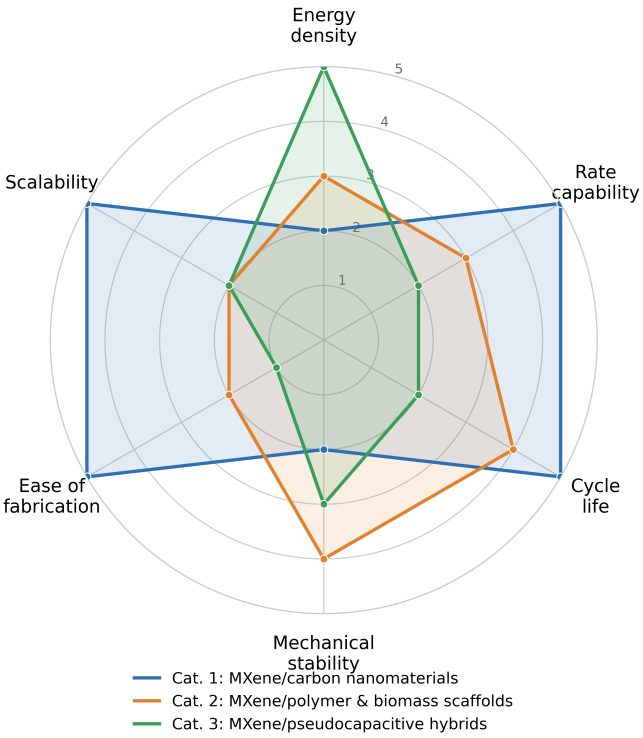


Figure 7. Radar-chart comparison of the three types of 3D MXene/carbon composites based on six performance dimensions. For all axes, larger values indicate more favorable characteristics. The plotted scores represent relative trends rather than absolute values.

Table 4. Performance comparison of representative 3D MXene/carbon composite electrodes.

Cat./ Ref	Composite	Preparation method	Electrolyte	Voltage window	Mass loading	Capacitance	Energy density	Cycling (retention@cycles)
1[50]	MXene/rGO aerogel	Ascorbic-acid self-assembly	1 M H_2SO_4	-0.2-1.0 V	-	233 F g^{-1} (1 A g^{-1})	-	91.0%@10,000
1[56]	MXene/rGO Zn-ion hybrid	Self-assembly	2 M $ZnSO_4$ (aqueous Zn^{2+})	0.2-1.6 V	-	128.6 F g^{-1} (0.4 A g^{-1})	34.9 Wh kg^{-1} (279.9 W kg^{-1})	> 95%@75,000 (5 A g^{-1})
1[57]	CNT-interwoven MXene aerogel	Self-assembly	PVA/H_2SO_4 gel	0-0.6 V	-	410.7 mF cm^{-2} (0.8 mA cm^{-2})	-	91.2%@5,000

1[58]	S,N-rGO/MXene aerogel	Heteroatom doping + assembly	PVA-KOH gel	0-1.4 V	1.8 mg cm^{-2}	88.9 F g^{-1} (1 A g^{-1}, all-solid)	24.2 Wh kg^{-1} (1,400.6 W kg^{-1})	~100%@10,000 (solid)
1[61]	F-free MXene ($ZnCl_2$) /rGO	Molten-salt etch + compositing	PVA-KOH gel	0-1.4 V	1.8 mg cm^{-2}	158.6 F g^{-1}	33.3 Wh kg^{-1} (1 A g^{-1})	100%@20,000
1[62]	MXene/rGO (Zn^{2+}-gel + UV N-doping)	Gelation + UV treatment	2 M H_2SO_4	0-1.0 V	2.19 mg cm^{-2}	1,323 F cm^{-3} (vol.)	39.1 Wh L^{-1} (11.6 Wh kg^{-1})	96.4%@8,000
2[63]	MXene/BC paper	Paper-making + kirigami	H_2SO_4/PVA gel	0-0.6 V	~2.0 mg cm^{-2}	111.5 mF cm^{-2}	0.00552 mWh cm^{-2}	72.2%@5,000
2[64]	PDA-bridged MXene/graphene	PDA bridging	3 M KOH	0-1.0 V	2.5 mg cm^{-2}	485 mF cm^{-2} (0.5 mA cm^{-2})	33.25 μWh cm^{-2}	87.4%@5,000
2[65]	$Ti_3C_2T_x$/PVA-derived carbon	Freeze-dry + 400 °C carbonization	1 M H_2SO_4	0-1.0 V	-	348.14 F g^{-1} (2 mV s^{-1})	37.8 Wh kg^{-1} (1,800 W kg^{-1})	92.52%@10,000 (10 A g^{-1})
2[66]	MXene/CNF-PANI aerogel film	Vacuum filtration + *in situ* PANI polymerization	3 M H_2SO_4	-0.65 ~ 0.3 V	-	327 F g^{-1} (3 mA cm^{-2})	-	71.6%@3,000
2[67]	All-wood MXene electrode	Vacuum infill + Ni^{2+} crosslink	PVA/H_2SO_4 gel	0-0.6 V	-	930 mF cm^{-2} (0.5 mA cm^{-2})	23 μWh cm^{-2} (577 μW cm^{-2})	87%@5,000
3[68]	Co_3O_4/MXene/rGO	*In situ* reduction + anneal	6 M KOH	0-1.6 V	-	345 F g^{-1} (1 A g^{-1}); R_s (0.44 Ω)	8.25 Wh kg^{-1} (159.94 W kg^{-1})	85%@10,000 (3 A g^{-1})
3[69]	CoS@MXene/ N-carbon foam	One-pot annealing	KOH/PVA gel	0-1.45 V	-	250 F g^{-1} (1 A g^{-1})	10.66 Wh kg^{-1} (678.1 W kg^{-1})	80.39%@5,000
3[70]	$NiCo_2O_4$/MXene/rGO	LDH→oxide on scaffold	PVA-KOH gel	0-1.5 V	-	1,633 F g^{-1} (1 A g^{-1})	40.5 Wh kg^{-1} (1,125.1 W kg^{-1})	Stable 0-60% strain
3[71]	ZIF-67 Co_3O_4/TiO_2 /MXene	CMC co-gel + pyrolysis	3 M KOH	0-1.4 V	~2.5 mg cm^{-2}	481.7 F g^{-1} (1 A g^{-1})	48.4 Wh kg^{-1} (699.8 W kg^{-1})	85.3%@10,000
3[72]	MoO_{3-x}/MXene-TiO_2 /C-graphene	Hydrothermal + IL electrolyte	Ternary IL	0-2.6 V	-	353.8 F g^{-1} (1 A g^{-1})	28.3 Wh kg^{-1} (1,193 W kg^{-1})	75%@2,300 (2 A g^{-1})

rGO: reduced graphene oxide; CNT: carbon nanotube; UV: ultraviolet; PVA: polyvinyl alcohol; BC: bacterial cellulose; PDA: polydopamine; CNF: carbon nanofiber; PANI: polyaniline; LDH: layered double hydroxide; CMC: carboxymethyl cellulose; IL: ionic liquid.

Even so, working through these trade-offs by experiment alone is slow: the governing parameters, composition ratio, pore architecture, interlayer spacing, surface terminations, mechanical response, are interdependent, and adjusting one rarely leaves the others fixed. It is this coupling that motivates the data-driven methods of the next section.

4. Machine-Learning-Guided Design and Prediction

The performance of MXene/3D-carbon composite electrodes depends on many variables at once: composition ratio, pore hierarchy, interlayer spacing, surface terminations, electrolyte compatibility, and these variables interact in ways that are far from additive. Mapping such a space by experiment alone is not feasible, and it is precisely this coupling that limits simple, empirical design rules. ML offers a complementary route: by learning statistical relationships from existing experimental and computational data, it can speed up screening and surface structure–property correlations that earlier work had missed. In the studies surveyed here, ML has been applied to the same design variables treated in Section 2 and Section 3, and five uses recur. It has been used to screen the MXene-to-carbon ratio so that capacitance and conductivity are optimized together[73], and to tune structural parameters, building-block geometry, and through it, pore structure and interlayer spacing[74]. A further group of studies predicts electrochemical behavior, specific capacitance, rate capability, cycling stability, directly from compositional and structural descriptors[75], while others assess mechanical stability, such as the compressive modulus of 3D aerogels[74]. Feature-importance analysis, finally, has been used to single out the descriptors that matter most: etching route, specific surface area, surface terminations, and thereby guide the choice of experimental conditions. The case studies that follow show these uses across datasets of three characteristic sizes.

Shelake *et al.*[75] built a database of over 7,300 data points from the MXene SC literature and compared several regression methods; RF showed the best robustness on this heterogeneous dataset, accurately predicting specific capacitance and cycling stability. However, the models are limited by the fact that the database is dominated by $Ti_3C_2T_x$ made by a few etching methods, and many important structural details, such as electrode thickness, pore size, and true mass loading, are missing from the source papers. The corresponding workflow covers data collection, feature engineering, prediction, and experimental validation. Shariq *et al.*[73] focused instead on compositional optimization within a narrow system; by comparing multiple algorithms (multiple linear regression (MLR), support vector regression (SVR), RF, and ANN) on an MXene/graphene-nanoplatelet dataset, they showed that an ANN provided the best fit for well-defined experimental features and accurately predicted both the optimal mixing ratio and the long-term cycling retention. The four algorithms ranked as ANN > MLR > SVR > RF in terms of both R^2 and root mean square error, with RF performing markedly worse on this small, well-curated dataset than on the large heterogeneous database of Shelake *et al.* indicating that the relative ranking of algorithms shifts substantially with dataset characteristics. Rong *et al.*[74] turned to a property less frequently treated by ML in this field, the mechanical response of MXene/cellulose-nanofiber aerogels. Using only 34 experimental samples, an ANN captured the nonlinear dependence of compressive modulus on structural parameters and identified the configuration yielding a maximum modulus of 29 kPa among 540 input combinations; the authors emphasized that mechanical properties are highly sensitive to the physical parameters of the building blocks, and that the scarcity of high-throughput mechanical data remains a severe bottleneck for model training. To provide a clearer overview of the current progress and limitations of ML-guided MXene electrode design, Table 5 summarizes and compares the reported ML models, dataset sizes, input descriptors, target properties, and prediction accuracy from representative studies.

Table 5. Summary of representative machine-learning studies for MXene-based composite electrodes.

Ref.	ML Models	Dataset Size	Input Descriptors	Target Properties	Prediction Accuracy/Key Findings
[75]	RF, etc.	> 7,300 data points	Structural/compositional parameters, etching methods	Specific capacitance, cycling stability	RF showed the highest robustness and accuracy for large, heterogeneous literature datasets.
[73]	ANN, MLR, SVR, RF	~100 data points	MXene-to-carbon mixing ratio	Optimal mixing ratio, long-term cycling retention	ANN provided the best fit (highest R^2, lowest RMSE) for system-specific optimization.
[74]	ANN	34 experimental samples	Physical parameters of building blocks, MXene content window	Compressive modulu	Accurately captured non-linear dependence; identified the configuration for maximum modulus.

ML: machine learning; RF: random forest; ANN: artificial neural network; MLR: multiple linear regression; SVR: support vector regression; RMSE: root mean square error.

Taken together, these case studies indicate that the applicability of ML to MXene/carbon electrodes depends strongly on the granularity and consistency of the underlying data, corresponding to three typical data–algorithm pairing regimes. As a practical heuristic, macroscopic literature-scale datasets ($\gtrsim 10^3$ samples) favor tree-based ensembles such as RF and XGBoost, which tolerate missing features and mixed data types; narrowly defined, system-specific datasets (~10^2 samples) favor ANN-type models that exploit a smoother feature–property mapping; and very small datasets (tens of samples) require careful regularization, physically informed feature pre-selection, and transfer learning to avoid overfitting. Beyond pointwise prediction, feature-importance analysis (SHAP values or permutation importance) has been used to rank individual descriptors, MXene-to-carbon ratio, specific surface area, etching route, and has in several cases identified compositional regimes not previously explored by empirical trial-and-error; for instance, Rong *et al.* located a mechanical-property optimum within an MXene-content window of 0.2–0.6 through this approach. These results show that, in practice, ML functions as one stage of a closed design loop rather than as an endpoint: data-driven models first narrow the search space and propose candidate compositions or structural configurations, such as the optimal mixing ratio of Shariq *et al.*[73] or the maximum-modulus configuration of Rong *et al.*[74], which are then synthesized and validated by electrochemical and mechanical characterization, and the resulting data feedback to refine the models. It is this prediction→synthesis→verification→feedback cycle, rather than isolated prediction, that gives ML its practical value in MXene/3D-carbon design, reducing experimental cost and surfacing structure–property regimes that empirical screening had missed, while complementing, rather than replacing, electrochemical intuition.

Despite these demonstrations, the application of ML to MXene/3D-carbon electrode design remains at an early stage, and its reliability, interpretability, and transferability are constrained by several problems that recur across the literature. The most basic is a shortage of data. Standardized, high-quality datasets are scarce, and what does exist is dominated by $Ti_3C_2T_x$ prepared through only a few etching protocols, while some sub-domains are thinner still, mechanical data for 3D aerogels, for instance, amount to no more than a few dozen samples. Models trained on so little tend to overfit, and they quietly inherit the bias of the literature, performing

best on the chemistries that happen to be most represented. A second difficulty is that the physics is genuinely multiscale: composite performance is set by a cross-scale interplay that runs from atomic-level surface chemistry to macroscopic electrode architecture. Because characterization and reporting standards differ from group to group, several of the most physically meaningful descriptors, true mass loading, electrochemically active surface area, pore-size distribution, and defect density, are often absent from the training data, which weakens both generalization and physical interpretability. The choice of descriptors is rarely standardized either. Many models lean on compositional features that are easy to tabulate while leaving out the harder-to-measure structural ones, so the feature set may capture correlation rather than the underlying physical cause, and a model built this way can look accurate within one synthesis route yet fail once the route or the electrode format changes. The synthesis itself adds a further mismatch. MXene preparation is sensitive to small shifts in etching temperature, to residual impurities left after washing and delamination, and to ambient humidity during storage; these conditions are seldom reported in full, so they rarely make their way into current models, which is one concrete reason predicted and measured performance still diverge.

These limitations call for progress on two fronts, computational and experimental. On the computational side, physics-informed ML is promising. Embedding physical constraints, mass balance, ion-transport equations, and thermodynamic-stability limits, into the model lets it represent microstructural features that purely data-driven approaches miss. In the data-scarce regions that dominate this field, that often translates into better interpretability and more reliable predictions. Such models work best, though, when the underlying data are broad. Most current databases stop at conventional $Ti_3C_2T_x$; extending them to double-transition-metal carbides such as $Mo_2TiC_2T_x$, to nitride-based MXenes, and to non-titanium systems would give models a real chance to generalize across chemistries instead of overfitting the handful that are well represented. The experimental side matters just as much. Coupling ML with high-throughput experiments and with simulation at several scales, atomic-level surface-chemistry analysis, mesoscale ion-transport modeling by kinetic Monte Carlo or phase-field methods, and macroscopic finite-element mechanical modeling, is what eventually links a computational prediction to a material that can be made and measured. These directions are discussed further in Section 5.2.

5. Conclusion and Outlook

5.1 Summary of recent progress

This review has mapped recent progress on 3D carbon-based MXene composite electrodes for SCs along three connected threads: synthesis, composite architecture, and ML.

On the synthesis side, MXene etching has gradually moved away from the original, hazardous hydrofluoric-acid process toward routes that are both safer and easier to control at the termination level. The milder *in situ* generation method is one example; alongside it sits a fast-growing set of so-called green strategies, Lewis-acid molten-salt and electrochemical etching among them, which give finer control over surface chemistry and leave behind more of the electrochemically active oxygen terminations.

The composite architectures fall into three broad groups. Pure-carbon frameworks act as interlayer spacers that keep 2D MXene sheets from restacking and open up bicontinuous channels for fast ion and electron transport; the payoff is long cycle life, but the purely capacitive storage mechanism caps their energy density. Polymer- or biomass-derived carbon networks instead provide 3D structural support and add some capacitance through carbonization-induced defect engineering, though usually at the cost of more involved processing and a trade-off between structural and electrical performance. Hybrid structures take a different route: by pairing the carbon scaffold with transition-metal compounds, LDHs, or MOF derivatives, and using the scaffold to buffer stress, they marry the high theoretical capacity of battery-type materials with reasonable cycle life, pushing energy density past what pure-carbon systems can reach.

ML, finally, has turned out to be a useful tool for screening candidates and generating hypotheses. Tree-based ensembles on literature-scale datasets, ANNs on system-specific compositions, and purpose-built algorithms for mechanical prediction are all accelerating MXene-composite design, provided the algorithm is matched to the size of the dataset it is given.

5.2 Remaining challenges

Several challenges specific to 3D carbon-based MXene electrodes remain, and most of them trace back to a single underlying tension rather than to separate, isolated bottlenecks.

The design choices that help one property tend to hurt another. Dense packing raises volumetric capacitance but restricts ion access. Widening the pores and interlayer spacing restores ion transport, yet weakens the framework and lowers volumetric density. Adding pseudocapacitive components lifts energy density while shortening cycle life. And the gentler, more scalable processing that commercialization needs usually gives up the structural precision that high performance relies on. Because these effects are coupled, the real task is not to push any one metric to its limit but to balance them at once, something the usual one-variable-at-a-time experiments handle poorly, and that is much of why the data-driven and mechanism-aware approaches discussed below are worth pursuing.

3D structural design. Balancing ion transport and structural stability remains a central issue in MXene/carbon composite electrodes. Dense architectures favor high volumetric capacitance but often restrict electrolyte penetration, whereas open porous frameworks improve ion accessibility while sacrificing mechanical strength. Moreover, because the MXene–carbon interface is typically maintained by relatively weak non-covalent interactions, interfacial degradation rather than failure of the individual components frequently limits long-term stability. Therefore, enhancing interfacial coupling through covalent bonds or molecular linkers such as PDA, combined with the rational integration of 1D, 2D, and 3D structural motifs, represents a promising direction for optimizing both electrochemical performance and mechanical integrity.

Porosity control. Precise control over pore architecture remains a major challenge for current assembly strategies, which generally yield broad pore-size distributions and strongly coupled pore characteristics. Consequently, enhancing specific surface area often compromises ion transport efficiency. Although template-assisted and ice-templating methods offer improved control over anisotropic porous structures, achieving uniform and reproducible architectures at the scale of practical electrodes remains difficult.

Durability and long-term environmental stability. MXene oxidation and structural degradation of battery-type active materials are the primary factors limiting the long-term stability of MXene/carbon composites. The formation of insulating TiO_2 gradually deteriorates electrical conductivity, while repeated volume variations in pseudocapacitive components can cause particle pulverization and loss of interfacial contact. Achieving commercially viable shelf-lives and operational lifespans requires strict long-term environmental stability. Surface engineering, such as heteroatom doping and the substitution of -F terminations with -O or -OH groups, offers a promising means of improving oxidation resistance. Together with stronger interfacial interactions and robust encapsulation strategies, these strategies may help suppress active-material detachment and definitively halt oxidative degradation.

Scalable manufacturing and cost analysis. As Table 3 shows, the three assembly routes trade scalability against structural control: water-based self-assembly is the most industrially viable, *in situ* carbonization scales but is energy-intensive, and template-assisted routes give the finest control yet are the hardest to scale. To push these composites toward commercialization, a comprehensive cost analysis, factoring in precursor expenses, etchant recycling, and the transition to continuous manufacturing techniques (such as roll-to-roll or slot-die coating), is urgently needed. Because most of the environmental burden lies upstream in the fluoride waste of HF-based etching, a realistic near-term route pairs fluorine-free etching (Section 2) with water-based self-assembly that preserves hierarchical porosity, then relies on wide-voltage-window electrolytes to narrow the energy-density shortfall relative to batteries.

Electrode mass loading. Bridging the gap between laboratory research and commercialization also requires addressing mass loading. Most reported high performance in the literature is achieved at low mass loadings (< 2 mg cm^{-2}). For practical devices, thick electrodes with high areal mass loadings (typically > 10 mg cm^{-2}) are mandatory to ensure competitive device-level energy density. However, increasing the mass loading often exacerbates ion-diffusion sluggishness and mechanical degradation. Future designs must prioritize 3D architectures that maintain unblocked transport kinetics and structural integrity even at commercial thicknesses.

Future directions. Further progress will turn on more than new materials; it will also require better data and a firmer grasp of mechanism. Much of this is a matter of reporting discipline. When studies consistently state mass loading, electrode thickness, electrolyte composition, voltage window, and the basis used for capacitance calculations, results become reproducible and, in aggregate, far more useful as training data. Mechanistic insight can be sharpened in parallel through operando methods, *in situ* XRD, Raman spectroscopy, electrochemical dilatometry, which track how structure evolves and degrades over cycling in real time. Physics-informed ML, drawing on open databases that span a wider set of MXene chemistries, can then extend these gains to regimes where experimental data are still thin. The trajectory these point to is a gradual shift away from trial-and-error optimization toward design grounded in mechanism and reproducible data.

Declarations

Acknowledgements

The authors declare that an AI-based assistant (Claude, Anthropic) was used solely for language polishing to improve the readability and grammar of the English text during manuscript preparation. All research content, including the study scope and design, literature analysis, interpretation of results, conclusions, figures, and tables, is the authors' original work and was not generated using AI tools. The authors reviewed and edited all AI-assisted text and take full responsibility for the content of the manuscript.

Authors contribution

Mu B: Conceptualization, writing-original draft, writing-review & editing, visualization, formal analysis.
Hou Z: Investigation, formal analysis.
Shi S: Investigation, visualization.

Conflicts of interest

The authors declare no conflicts of interest.

Ethical approval

Not applicable.

Consent to participate

Not applicable.

Consent for publication

Not applicable.

Availability of data and materials

Not applicable.

Funding

This work was supported by the Guangxi Universities Young and Middle-aged Teachers' Research Basic Ability Improvement Project (Grant No. 2024KY0396).

Copyright

© The Author(s) 2026.

References

1. Bhaduri A, Kim CE, Ha TJ. Recent developments in materials design for advanced supercapacitors. Energy Environ Mater. 2025;8(6):e70070. [DOI]
2. Li C, Chen W, Xu X, Feng J, Li WY. Sunlight-driven azoswitches for solar thermal energy storage and release. Innov Mater. 2025;3(1):100110. [DOI]
3. Liu L, Qin X, Zhang R. Advanced carbon electrodes for supercapacitors: Design strategies, performance optimization, and practical applications. Smart Mater Devices. 2025;1(2):202504. [DOI]
4. Kariachan S, Shibu J, Velayudhan P, Sidharthan SK, Velayudhan P, Simon SM, et al. Exploring the advances in 2D materials as a quest for energy storage electrode materials. RSC Adv. 2026;16(12):10847-10886. [DOI]
5. Tang Y, Bi Z, Xie Y, Xuan X, Yang C. Two-dimensional vacancy-doped MXene nanomaterials for supercapacitors. Front Chem. 2025;13:1656521. [DOI]
6. Naguib M, Kurtoglu M, Presser V, Lu J, Niu J, Heon M, et al. Two-dimensional nanocrystals produced by exfoliation of Ti_3AlC_2. Adv Mater. 2011;23(37):4248-4253. [DOI]
7. Pang J, Zhang S, Rümmeli MH, Liu H, Zhou W. Evolving MXene species. Innov Mater. 2023;1(2):100027. [DOI]
8. Xiang M, Shen Z, Zheng J, Song M, He Q, Yang Y, et al. Gas-phase synthesis of Ti_2CCl_2 enables an efficient catalyst for lithium-sulfur batteries. Innovation. 2024;5(1):100540. [DOI]
9. De Leuze O, Fernandes FM, Arib S, Caputo L, Fontes AP, Nguyen VH, et al. Anisotropic charge transport in 2D single crystals of $Ti_3C_2T_x$ MXenes. Commun Mater. 2025;6(1):186. [DOI]
10. Yue Y, Liu N, Su T, Cheng Y, Liu W, Lei D, et al. Self-powered nanofluidic pressure sensor with a linear transfer mechanism. Adv Funct Mater. 2023;33(13):2211613. [DOI]
11. Xu L, Iqbal R, Wang Y, Taimoor S, Hao L, Dong R, et al. Emerging two-dimensional materials: Synthesis, physical properties, and application for catalysis in energy conversion and storage. Innov Mater. 2024;2(1):100060. [DOI]
12. Lv K, Zhang J, Zhao X, Kong N, Tao J, Zhou J. Understanding the effect of pore size on electrochemical capacitive performance of MXene foams. Small. 2022;18(27):e2202203. [DOI]
13. Abbas SZ, Vikraman D, Sheikh ZA, Ali S, Hussain I, Goak JC, et al. Improving the electrochemical properties of MXene through intercalation of WC and TiC nanoparticles for supercapacitors application. J Colloid Interface Sci. 2025;696:137845. [DOI]
14. Gao T, Lai CW, Rangappa SM, Siengchin S, Gapsari F, Li Y, et al. MXene-based materials for supercapacitors: Trends and opportunities. J Mater Sci Mater Electron. 2025;36(29):1877. [DOI]
15. Kumar J, Tan J, Soomro RA, Sun N, Xu B. Probing the synergistic effects of amino compounds in mitigating oxidation in 2D $Ti_3C_2T_x$ MXene nanosheets in aqueous environments. Chem Sci. 2025;16(4):1986-1994. [DOI]
16. Marquez KP, Sisican KMD, Ibabao RP, Malenab RAJ, Judicpa MAN, Henderson L, et al. Understanding the chemical degradation of $Ti_3C_2T_x$ MXene dispersions: A chronological analysis. Small Sci. 2024;4(10):2400150. [DOI]
17. Kota S, Divya BN, Acharya NS, Kumar SGP, Annapragada R. MXene-based nanomaterials for high-performance supercapacitors. Discov Electron. 2026;3(1):12. [DOI]
18. Li K, Liang M, Wang H, Wang X, Huang Y, Coelho J, et al. 3D MXene architectures for efficient energy storage and conversion. Adv Funct Mater. 2020;30(47):2000842. [DOI]

19. Yang F, Lv K, Zhao X, Kong D, Kong N, Luo Z, et al. Hierarchical heterostructures of MXene and mesoporous hollow carbon sphere for improved ion accessibility and rate performance. Chem Eng J. 2024;494:153246. [DOI]
20. Chen X. Nature-inspired aerogel fiber. Innov Mater. 2024;2(2):100070. [DOI]
21. Wang S, Yu L, Jia X, Zhang L, Liu H, Gao E, et al. Cellulose nanofibril-guided orienting response of supramolecular network enables superstretchable, robust, and antifatigue hydrogel. Innov Mater. 2024;2(4):100092. [DOI]
22. Niu X, He Y, Musl O, Bautista GFM, Xie Q, Wu Y, et al. Bark extractives as sources of carbon-efficient functional precursors and materials. Innov Mater. 2024;2(2):100074. [DOI]
23. Zhang B, Qiang G, Barta K, Sun Z. Bio-based polymers from lignin. Innov Mater. 2024;2(2):100062. [DOI]
24. Zhao H, Hu GC, Abraham B, Wang Q, Zhong N, Shen F, et al. A sustainable cellulose bioplastic film with extraordinary mechanical performance regenerated by vapor-induced phase separation. Innov Mater. 2025;3(2):100133. [DOI]
25. Wang M, Hong Y, He W, Zhang Q, Yu G, Liu J, et al. Nature-inspired MXene electrode with the highly interconnected gradient nanoconfined architecture. Adv Mater. 2025;37(45):e11444. [DOI]
26. Park W, Noh J, Gu GH, Nam G, Jung SM, Kim YT, et al. Machine learning-enabled fast exploration of stable and active single-atom catalysts for oxygen evolution reaction. Innov Mater. 2024;2(2):100072. [DOI]
27. Shang Y, Zhou Z, Han R, Wang H, Liu X, Yang Y. Customized design of amorphous solids by generative deep learning. Innov Mater. 2024;2(2):100071. [DOI]
28. Ma H, Jiao Y, Guo W, Liu X, Li Y, Wen X. Machine learning predicts atomistic structures of multielement solid surfaces for heterogeneous catalysts in variable environments. Innovation. 2024;5(2):100571. [DOI]
29. Cai G, Cao Z, Xie F, Jia H, Liu W, Wang Y, et al. Predicting structure-dependent Hubbard U parameters *via* machine learning. Mater Futur. 2024;3(2):025601. [DOI]
30. Wines D, Choudhary K. Data-driven design of high pressure hydride superconductors using DFT and deep learning. Mater Futur. 2024;3(2):025602. [DOI]
31. Shavita , Sharma S, Sharma AL, Singh S. Machine learning models for predicting electrochemical behavior of MXene for energy storage applications. J Power Sources. 2026;670:239514. [DOI]
32. Poh WS, Yiang WJ, Ong WJ, Show PL, Foo CY. Enhancing MXene-based supercapacitors: Role of synthesis and 3D architectures. J Energy Chem. 2024;91:1-26. [DOI]
33. Aravind AM, Tomy M, Kuttapan A, Kakkassery Aippunny AM, Suryabai XT. Progress of 2D MXene as an electrode architecture for advanced supercapacitors: A comprehensive review. ACS Omega. 2023;8(47):44375-44394. [DOI]
34. Krishna Paul T, Parvez MS, Mashfik Ahmed C. Recent progress and prospects of MXene/cellulose-based composite electrodes: A sustainable pathway towards supercapacitor application. ChemElectroChem. 2024;11(2):e202300435. [DOI]
35. Prabhakar Vattikuti SV, Shim J, Rosaiah P, Mauger A, Julien CM. Recent advances and strategies in MXene-based electrodes for supercapacitors: Applications, challenges and future prospects. Nanomaterials. 2023;14(1):62. [DOI]
36. Gogotsi Y, Huang Q. MXenes: Two-dimensional building blocks for future materials and devices. ACS Nano. 2021;15(4):5775-5780. [DOI]
37. Naguib M, Mashtalir O, Carle J, Presser V, Lu J, Hultman L, et al. Two-dimensional transition metal carbides. ACS Nano. 2012;6(2):1322-1331. [DOI]
38. Ghidiu M, Lukatskaya MR, Zhao MQ, Gogotsi Y, Barsoum MW. Conductive two-dimensional titanium carbide 'clay' with high volumetric capacitance. Nature. 2014;516(7529):78-81. [DOI]
39. Jin Y, Geng J, Wang Y, Zhao Z, Chen Z, Guo Z, et al. Flexible all-solid-state asymmetric supercapacitor based on $Ti_3C_2T_x$ MXene/graphene/carbon nanotubes. Surf Interfaces. 2024;53:104999. [DOI]
40. Chien CC, Liu YH, Luo KH, Liu TY, Kao YT, Yang SH, et al. Polyaniline/Ti_3C_2 MXene composites with artificial 3D biomimetic surface structure of natural macaw feather applied for anticorrosion coatings. Biomimetics. 2025;10(7):465. [DOI]
41. Li Y, Shao H, Lin Z, Lu J, Liu L, Duployer B, et al. A general Lewis acidic etching route for preparing MXenes with enhanced electrochemical performance in non-aqueous electrolyte. Nat Mater. 2020;19(8):894-899. [DOI]
42. Liu L, Orbay M, Luo S, Duluard S, Shao H, Harmel J, et al. Exfoliation and delamination of $Ti_3C_2T_x$ MXene prepared *via* molten salt etching route. ACS Nano. 2022;16(1):111-118. [DOI]
43. Li T, Yao L, Liu Q, Gu J, Luo R, Li J, et al. Fluorine-free synthesis of high-purity $Ti_3C_2t_x$ (T=OH, O) via alkali treatment. Angew Chem Int Ed. 2018;57(21):6115-6119. [DOI]
44. Li G, Tan L, Zhang Y, Wu B, Li L. Highly efficiently delaminated single-layered MXene nanosheets with large lateral size. Langmuir. 2017;33(36):9000-9006. [DOI]
45. Kulkarni M, Lalic A, Balu R, Zhang H, Dutta NK, Roy Choudhury N. Hydrothermal synthesis of MXenes in alkali environment and development of MXene/PEDOT: PSS composite electrodes for supercapacitor applications. MRS Adv. 2024;9(17):1310-1317. [DOI]
46. Guo Y, Zhang X, Jin S, Xia Q, Chang Y, Wang L, et al. Synthesis of Mo_2C MXene with high electrochemical performance by alkali hydrothermal etching. J Adv Ceram. 2023;12(10):1889-1901. [DOI]
47. Yang S, Zhang P, Wang F, Ricciardulli AG, Lohe MR, Blom PWM, et al. Fluoride-free synthesis of two-dimensional titanium carbide (MXene) using a binary aqueous system. Angew Chem Int Ed. 2018;57(47):15491-15495. [DOI]
48. Liu L, Zschiesche H, Antonietti M, Gibilaro M, Chamelot P, Massot L, et al. *In situ* synthesis of MXene with tunable morphology by electrochemical etching of MAX phase prepared in molten salt. Adv Energy Mater. 2023;13(7):2203805. [DOI]
49. Yin T, Li Y, Wang R, Al-Hartomy OA, Al-Ghamdi A, Wageh S, et al. Synthesis of $Ti_3C_2F_x$ MXene with controllable fluorination by

electrochemical etching for lithium-ion batteries applications. Ceram Int. 2021;47(20):28642-28649. [DOI]
50. Shao L, Xu J, Ma J, Zhai B, Li Y, Xu R, et al. MXene/RGO composite aerogels with light and high-strength for supercapacitor electrode materials. Compos Commun. 2020;19:108-113. [DOI]
51. Sun L, Su X, Chen Y, Zhuo K, Li H, Sun D, et al. Ferric ion-assisted assembly of MXene/TiO_2-graphene aerogel for ionic liquid-based supercapacitors. Chem Eng J. 2023;476:146731. [DOI]
52. Yan J, Ren CE, Maleski K, Hatter CB, Anasori B, Urbankowski P, et al. Flexible MXene/graphene films for ultrafast supercapacitors with outstanding volumetric capacitance. Adv Funct Mater. 2017;27(30):1701264. [DOI]
53. Lu Y, Bai J, Sun B, Li N, Wang C, Yang Z, et al. An MXene/poly(vinyl alcohol)/reduced graphene oxide nanocomposite aerogel as an ultra-stable electrode for capacitive storage. ACS Appl Nano Mater. 2025;8(26):13296-13307. [DOI]
54. Liu Y, Wang D, Zhang C, Zhao Y, Ma P, Dong W, et al. Compressible and lightweight MXene/carbon nanofiber aerogel with "layer-strut" bracing microscopic architecture for efficient energy storage. Adv Fiber Mater. 2022;4(4):820-831. [DOI]
55. Li M, Zhao S, Wei F, Shen Y, Ma ZF. Electrostatic self-assembly to construct MXene@PS@CF_x electrode for high power density lithium primary cells. Small. 2025;21(15):e2412387. [DOI]
56. Wang Q, Wang S, Guo X, Ruan L, Wei N, Ma Y, et al. MXene-reduced graphene oxide aerogel for aqueous zinc-ion hybrid supercapacitor with ultralong cycle life. Adv Elect Materials. 2019;5(12):1900537. [DOI]
57. Xu T, Wang Y, Liu K, Zhao Q, Liang Q, Zhang M, et al. Ultralight MXene/carbon nanotube composite aerogel for high-performance flexible supercapacitor. Adv Compos Hybrid Mater. 2023;6(3):108. [DOI]
58. Liu X, Lu Z, Huang X, Bai J, Li C, Tu C, et al. Self-assembled S, N co-doped reduced graphene oxide/MXene aerogel for both symmetric liquid- and all-solid-state supercapacitors. J Power Sources. 2021;516:230682. [DOI]
59. Kumar S, Rehman MA, Lee S, Kim M, Hong H, Park JY, et al. Supercapacitors based on $Ti_3C_2T_x$ MXene extracted from supernatant and current collectors passivated by CVD-graphene. Sci Rep. 2021;11(1):649. [DOI]
60. Kim SK, Kim SA, Han YS, Jung KH. Supercapacitor performance of MXene-coated carbon nanofiber electrodes. . 2024;10(2):32. [DOI]
61. Ren F, Lu Z, Liu X, Wang T, Huang X, Dou J, et al. Lewis acid-etched MXene self-assembled with reduced graphene oxide for symmetrical supercapacitors with liquid/solid electrolytes. J Alloys Compd. 2024;978:173480. [DOI]
62. Zhao H, Shen H, Cai M, Xu J, Li L, Liu S, et al. Synergistic 3D network eengineering and surface terminal regulation in MXene/graphene aerogels with ultrahigh volumetric capacitance and rate-capability for supercapacitors. Chem Eng J. 2025;523:168552. [DOI]
63. Jiao S, Zhou A, Wu M, Hu H. Kirigami patterning of MXene/bacterial cellulose composite paper for all-solid-state stretchable micro-supercapacitor arrays. Adv Sci. 2019;6(12):1900529. [DOI]
64. Wang Y, Deng Z, Ou H, Feng S, Xiang X. Polydopamine-bridged MXene/graphene composite aerogel for bifunctional applications in supercapacitors and piezoresistive sensors. Chem Eng J. 2025;522:167528. [DOI]
65. Lu Y, Bai J, Sun B, Li N, Yang Z, Yu H, et al. Enhancing the capacitive energy storage ability of $Ti_3C_2T_x$ MXene and PVA-derived carbon composite aerogels through structural disorder. Electrochim Acta. 2025;521:145910. [DOI]
66. Xu L, Wang W, Liu Y, Liang D. Nanocellulose-linked MXene/polyaniline aerogel films for flexible supercapacitors. Gels. 2022;8(12):798. [DOI]
67. Chen W, Yang K, Luo M, Zhang D, Li Z, Liu C, et al. Carbonization-free wood electrode with MXene-reconstructed porous structure for all-wood eco-supercapacitors. EcoMat. 2023;5(1):e12271. [DOI]
68. Liu R, Zhang A, Tang J, Tian J, Huang W, Cai J, et al. Fabrication of cobaltosic oxide nanoparticle-doped 3 D MXene/graphene hybrid porous aerogels for all-solid-state supercapacitors. Chemistry. 2019;25(21):5547-5554. [DOI]
69. Liao L, Zhang A, Zheng K, Liu R, Cheng Y, Wang L, et al. Fabrication of cobaltous sulfide nanoparticle-modified 3D MXene/carbon foam hybrid aerogels for all-solid-state supercapacitors. ACS Appl Mater Interfaces. 2021;13(24):28222-28230. [DOI]
70. Zhang M, Jiang D, Jin F, Sun Y, Wang J, Jiang M, et al. Compression-tolerant supercapacitor based on $NiCo_2O_4$/$Ti_3C_2T_x$ MXene/reduced graphene oxide composite aerogel with insights from density functional theory simulations. J Colloid Interface Sci. 2023;636:204-215. [DOI]
71. Xu H, Hu Q, Zhao T, Zhu J, Lian Z, Jin X. Sodium carboxymethylcellulose/MXene/zeolite imidazolium framework-67-derived 3D porous carbon aerogel for high-performance asymmetric supercapacitors. Carbohydr Polym. 2024;326:121641. [DOI]
72. Jing L, Chen Y, Sun L, Zhuo K, Sun D, Su X, et al. MoO_{3-x}-assisted MXene-derived TiO_2/C-graphene composite structure for high-capacitance electrode materials of ionic liquid-based supercapacitors. J Energy Storage. 2025;133:118034. [DOI]
73. Shariq M, Marimuthu S, Dixit AR, Chattopadhyaya S, Pandiaraj S, Muthuramamoorthy M, et al. Machine learning models for prediction of electrochemical properties in supercapacitor electrodes using MXene and graphene nanoplatelets. Chem Eng J. 2024;484:149502. [DOI]
74. Rong C, Zhou L, Zhang B, Xuan FZ. Machine learning for mechanics prediction of 2D MXene-based aerogels. Compos Commun. 2023;38:101474. [DOI]
75. Shelake AR, Karade VC, Selvaraj M, Assiri MA, More DD, Patil AD, et al. Machine learning-guided optimization, predictive modeling, and experimental validation of MXene-based supercapacitors. J Power Sources. 2026;663:238863. [DOI]

Publisher's Note

Science Exploration remains a neutral stance on jurisdictional claims in published maps and institutional affiliations. The views expressed in this article are solely those of the author(s) and do not reflect the opinions of the Editors or the publisher.